JARO 16: 547–567 (2015)
DOI: 10.1007/s10162-015-0531-y

JARO
Journal of the Association for Research in Otolaryngology

Research Article

Finite-Element Modelling of the Response of the Gerbil Middle Ear to Sound

Nima Maftoon,[1] W. Robert J. Funnell,[1,2] Sam J. Daniel,[3,2] and Willem F. Decraemer[4]

[1]*Department of BioMedical Engineering, McGill University, 3775 rue University, Montréal, QC H3A 2B4, Canada*

[2]*Department of Otolaryngology—Head and Neck Surgery, McGill University, Montréal, QC, Canada*

[3]*Department of Pediatric Surgery, McGill University, Montréal, QC, Canada*

[4]*Biomedical Physics, University of Antwerp, Antwerp, Belgium*

Received: 26 May 2014; Accepted: 15 June 2015; Online publication: 22 July 2015

ABSTRACT

We present a finite-element model of the gerbil middle ear that, using a set of baseline parameters based primarily on a priori estimates from the literature, generates responses that are comparable with responses we measured in vivo using multi-point vibrometry and with those measured by other groups. We investigated the similarity of numerous features (umbo, pars-flaccida and pars-tensa displacement magnitudes, the resonance frequency and break-up frequency, etc.) in the experimental responses with corresponding ones in the model responses, as opposed to simply computing frequency-by-frequency differences between experimental and model responses. The umbo response of the model is within the range of variability seen in the experimental data in terms of the low-frequency (i.e., well below the middle-ear resonance) magnitude and phase, the main resonance frequency and magnitude, and the roll-off slope and irregularities in the response above the resonance frequency, but is somewhat high for frequencies above the resonance frequency. At low frequencies, the ossicular axis of rotation of the model appears to correspond to the anatomical axis but the behaviour is more complex at high frequencies (i.e., above the pars-tensa break-up). The behaviour of the pars tensa in the model is similar to what is observed experimentally in terms of magnitudes, phases, the break-up frequency of the spatial vibration pattern, and the bandwidths of the high-frequency response features. A sensitivity analysis showed that the parameters that have the strongest effects on the model results are the Young's modulus, thickness and density of the pars tensa; the Young's modulus of the stapedial annular ligament; and the Young's modulus and density of the malleus. Displacements of the tympanic membrane and manubrium and the low-frequency displacement of the stapes did not show large changes when the material properties of the incus, stapes, incudomallear joint, incudostapedial joint, and posterior incudal ligament were changed by ±10 % from their values in the baseline parameter set.

Keywords: tympanic membrane, pars tensa, pars flaccida, vibration, ossicles, sound stimulus, dynamic model, frequency response, sensitivity analysis

INTRODUCTION

Models of the middle ear have proven to be important for understanding its function and for predicting its response to pathological changes, diagnostic tests and treatment methods, and they are indispensable for developing surgical simulators. Different approaches to modelling the middle ear were recently reviewed by Funnell et al. (2012, 2013). In finite-element (FE) models that are based on the detailed anatomical and biomechanical properties of the middle-ear structures, the model parameters are fundamentally con-

Correspondence to: W. Robert J. Funnell · Department of BioMedical Engineering · McGill University · 3775 rue University, Montréal, QC H3A 2B4, Canada. Telephone: +1-514-398-6739; email: robert.funnell@mcgill.ca; URL: http://audilab.bme.mcgill.ca

nected to the physiological characteristics of the system. With increasing accessibility of FE preprocessing programmes and solvers, this method has been increasingly applied in modelling of the middle ear. Most middle-ear FE models have been developed for the human middle ear, starting with Wada et al. (1992), but higher-quality experimental data are available for validating the models that have been developed for other species, including cat (e.g., Funnell and Laszlo 1978; Ladak and Funnell 1996; Tuck-Lee et al. 2008), rabbit (Aernouts et al. 2010) and rat (Hesabgar et al. 2010; Ghadarghadar et al. 2013). Gerbils are widely used in auditory research and therefore a wealth of knowledge is available concerning their auditory system (see Maftoon et al. 2013, for some references). The middle ear of this species has been the subject of a number of FE studies. Funnell et al. (1999, 2000) presented some preliminary model results for low frequencies and the model was later refined by Elkhouri et al. (2006). (The latter model was developed for low frequencies and did not include either inertia or damping effects; differences between it and the present model are described here in footnotes where appropriate, and the low-frequency results of the two models are compared in the "Model Parameters" section.) Material characterization was done using FE modelling in conjunction with pressurization by Decraemer et al. (2010) for the pars flaccida, and in conjunction with indentation data by Aernouts and Dirckx (2011, 2012) for the pars flaccida and pars tensa, respectively. Decraemer et al. (2011) used FE modelling to study the effects of tympanic-membrane (TM) geometrical asymmetry on ossicle-motion asymmetry in response to positive and negative static pressures. Maftoon et al. (2011) presented some preliminary modelling results on the response of the gerbil middle ear at audio frequencies. The latter study is extended by the present work.

We investigated the similarity of several features in the experimental responses to corresponding features in the model responses. These features include the displacement magnitudes of the umbo and pars flaccida at frequencies well below the middle-ear resonance and at the resonance; the ratio of the umbo magnitude at the resonance to that at frequencies well below resonance; the middle-ear resonance frequency; the full width at half maximum of the umbo velocity response; the shallow maximum and shallow minimum in the manubrium and pars-tensa responses due to a pars-flaccida contribution; the bandwidth, magnitude and phase changes of irregularities in the umbo response above the middle-ear resonance; the pars-flaccida roll-off beyond its resonance; the manubrial vibration modes; the umbo-to-lateral-process displacement magnitude ratio; the pars-tensa break-up frequency; the bandwidths of features in the pars-tensa responses above the break-up frequency; the ossicular lever ratio; and the piston-like component of stapes displacement.

MATERIALS AND METHODS

Geometry, Model Components and Mesh

The FE model used in this study is shown in Figure 1. The 3-D geometry of the model is a refinement of the one used by Decraemer et al. (2011) and is based on segmentation of a microCT dataset, supplemented by histological images. The geometry of the posterior incudal ligament was based on the orthogonal-plane fluorescence optical sectioning (OPFOS) data of Buytaert et al. (2011). The model includes the pars tensa, pars flaccida, malleus, incus, stapes, posterior incudal ligament, stapedial annular ligament, incudomallear joint and incudostapedial joint, as well as a representation of the cochlear load. In-house FE preprocessing software[1] (Fie, Tr3 and Fad) was used to perform image segmentation and surface triangulation and to prepare unstructured surface meshes for volume mesh generation using the open-source software Gmsh (Geuzaine and Remacle 2009). The triangles of the surface meshes, and thus the tetrahedra of the volume meshes, were made smaller where necessary to represent small geometric details, such as details in the incudostapedial joint, stapes head and stapedial annular ligament, as seen in Figure 1A. The FE solver was Code_Aster[2] version 11.3, which is also open-source. Simulations were done on the supercomputer Guillimin of McGill University. Guillimin is a cluster of Intel Westmere EP Xeon X5650 and Intel Sandy Bridge EP E5-2670 processors running under the CentOS 6 distribution of Linux. The baseline study was performed using one processor and 8 GB of RAM. Sensitivity analyses were typically done using six processors, each using 20 GB of RAM, in a Code_Aster parametric-study session. This launched six instances of the simulation in parallel. Each simulation for one set of parameters took about an hour.

The TM was modelled using seven-node second-order *TRIA7 COQUE_3D* shell elements. In this element type, each node possesses three translational and three rotational degrees of freedom, except for the centre node which possesses only three rotational degrees of freedom. Kuypers et al. (2005) reported thicknesses along four lines across the pars tensa in the gerbil. An interpolation algorithm (which will be described in a subsequent paper) has been developed to reconstruct a thickness map for the entire pars-tensa surface from their

[0] http://audilab.bme.mcgill.ca/AudiLab/sw/
[0] http://code-aster.org/

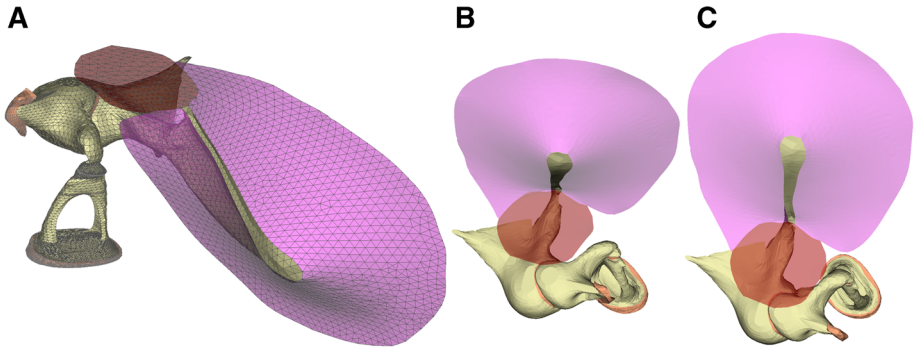

Fig. 1. Reconstructed 3-D model of gerbil middle ear used in finite-element analysis. **A** A posterolateral view of all components of the model; **B** and **C** two views of the tympanic membrane as seen from extreme angles through the ear canal in our experimental measurements (Maftoon et al. 2013, 2014). The TM is shown as semi-transparent.

measurements. For each of the four lines, a spatially varying average across all of the ears measured by Kuypers et al. was used. The algorithm generates a baseline variable thickness in the range of 5 to 38 μm. For the pars flaccida, Kuypers et al. (2005) found a thickness distribution that is irregular; for simplicity, we used a constant thickness of 23.5 μm (their reported mean) for the pars flaccida in our model.

Ten-node second-order *TETRA10 3D* tetrahedral solid elements were used to model the ossicular chain. Each node of this element type possesses three translational degrees of freedom and no rotational degrees of freedom. In order to ensure correct coupling between the shell elements of the TM and the 3-D solid elements of the malleus, the pars tensa was continued over the lateral surface of the manubrium and nodes were shared between the two structures.[3] As described by Rosowski et al. (1999), in the gerbil the malleus is connected to the cavity anteriorly by a bony attachment (Fig. 2).[4]

The ossicular ligaments and joints were modelled using ten-node second-order *TETRA10 3D_INCO* tetrahedral incompressible solid elements. This is a special element, with a three-field (displacement, pressure and volumetric strain) mixed formulation, designed to correctly model the behaviour of nearly incompressible materials. Like the elements used for the ossicles, these elements have only translational degrees of freedom. The posterior incudal ligament surrounds the posterior end of the short process of the incus, as seen in the histological image shown in Figure 3 and as reported by Buytaert et al. (2011) using OPFOS.[5] Buytaert et al. (2011) reported that the synovial nature of the incudomallear joint "is not confirmed from" their OPFOS or μCT data and that "no fluid or open space is detected in the joint cleft". Considering the resolution of these methods, their observation is not unexpected. Even in histological images, the synovial cleft is sometimes not obvious because the bones have been pushed together. Figure 4 shows histological images of the gerbil incudomallear and incudostapedial joints in which the synovial clefts are clearly visible. For simplicity, the joints were assumed to be elastic solids and details of the synovial fluid, cartilage and joint capsule were not modelled.

Boundary Conditions

The pars tensa was considered to be fully clamped around its periphery (i.e., all of the six degrees of freedom were set to zero). The pars flaccida was considered to be simply supported around its periph-

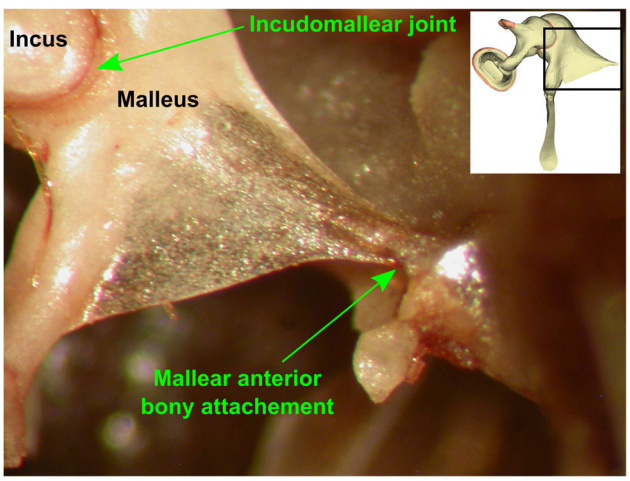

Fig. 2. Anterior mallear bony attachment in gerbil ear. The *inset in the top right corner* shows a view of the model in the orientation as seen in the photograph. The *black frame in the inset* shows the frame of the image. Unlike the case in human, the anterior process of the malleus is long and is attached directly to the bony cavity wall by a thin bony attachment (Rosowski et al 1999).

[0] In the previous gerbil model from our group (Elkhouri et al. 2006), based on magnetic-resonance-microscopy images, the inferior part of the manubrium was narrower than it should have been.
[0] Instead of this bony attachment, Elkhouri et al. (2006) used a ligament to connect the malleus to the cavity wall.
[0] In the model by Elkhouri et al. (2006), this ligament was considered to be composed of two bundles.

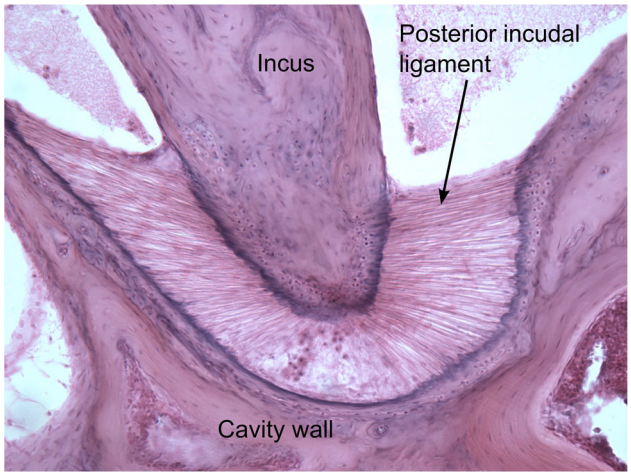

Fig. 3. Histology of posterior incudal ligament in the gerbil middle ear (courtesy of Clarinda Northrop). The posterior incudal ligament in the gerbil surrounds the posterior end of the short process of the incus.

ery (i.e., the three translational degrees of freedom were set to zero but the rotational degrees of freedom were not), as suggested by Gea et al. (2009). It shared nodes (and all of the six degrees of freedom of shell elements) with the pars tensa at their interface.

Fay et al. (2006) modelled the open middle-ear cavity as a radiation impedance but did not comment on the magnitude of the effect. If the radiation impedance of the TM is modelled as the radiation impedance of a piston in an infinite baffle (Beranek 1954, p. 124 ff.; Kinsler et al. 1999, p. 186 ff.) the real part of the impedance (the series resistance) will be less than 3000 Pa s/m^3 for the gerbil in the frequency range of 200 to 10,000 Hz. This value is negligible compared with the resistance of 6.6×10^7 Pa s/m^3 estimated by Teoh et al. (1997) for the TM, ossicles and cochlear complex in gerbils. Moreover, according to Rabbitt and Holmes (1988, Fig. 4) the effect would seem to be relatively small below 10 kHz for a small TM like that of the gerbil. As an approximation to the open-cavity condition, the radiation impedance is neglected here for simplicity, as has often been done.

For the ligaments and the anterior mallear bony attachment, all three translational degrees of freedom were set to zero for the nodes where they would be attached to the cavity wall, which was not explicitly included in the model.[6]

Calculation of Frequency Responses

ProcedureFrequency responses were calculated following the procedure suggested by Funnell et al. (1987), by applying a unit-step sound pressure of 1 Pa on the TM surface and performing transient FE analyses. The direct implicit time-integration scheme of Newmark (1959) was employed. The two parameters β and γ of this method were set to 0.25 and 0.5, respectively, to provide an unconditionally stable solution as suggested by Newmark. (These parameters are not related to the Rayleigh damping parameters α and β discussed in the "Damping" section.) Simulations were continued for 50 ms after the onset of the unit-step sound-pressure function. Frequency responses were obtained by differentiating the step responses and then computing the fast Fourier transforms of the resulting impulse responses. Our frequency resolution of 12 Hz allowed us to successfully perform phase unwrapping by adding multiples of cycles when absolute jumps between consecutive bins are greater than or equal to half a cycle. After unwrapping, the maximum phase jump between two frequency bins was only 77°, confirming that the frequency resolution was adequate. We also checked the configuration and continuity of the Nyquist plots as described in the Appendix of Maftoon et al. (2013). As in our report of experimental measurements (Maftoon et al. 2013), we define the break-up frequency of the pars tensa as the frequency at which the phase divergence of the points is more than 15°. Since the main purpose of this paper is to validate the model results against the multi-point experimental data of Maftoon et al. (2013, 2014), we chose to greatly reduce the computation time by not computing frequency responses for all of the ~84,000 nodes in the model. Instead, we processed only nodes corresponding to where we made experimental measurements: a row of nodes along the manubrium, a row of nodes on the pars tensa on a line perpendicular to the manubrium midway along its length, and a node at the centre of the pars flaccida. To permit comparison with stapes data in the literature, we also processed a node at the centre of the stapes footplate.

We assumed a uniform sound pressure field in the ear canal for the frequencies covered in this article (below 10 kHz), consistent with the observations of Bergevin and Olson (2014) in gerbils. To model the open-cavity condition, we assumed zero sound pressure in the middle-ear cavity. These frequently made assumptions allowed us to greatly reduce the complexity of the model by avoiding modelling of the acoustic fields in the ear canal and middle-ear cavity. Displacement results were normalized by the sound pressure in the ear canal. We have previously proposed a method for estimating ideal open-cavity responses from measurements with partial openings in the cavity wall (Maftoon et al. 2014). In this paper, we use that method to compare our no-cavity modelling results with experimental results. The

[6] In the model of Elkhouri et al. (2006) the stapedial annular ligament was modelled by shell elements and the rotational degrees of freedom of its nodes were fixed by mistake. That boundary condition allowed only piston-like motion of the stapes.

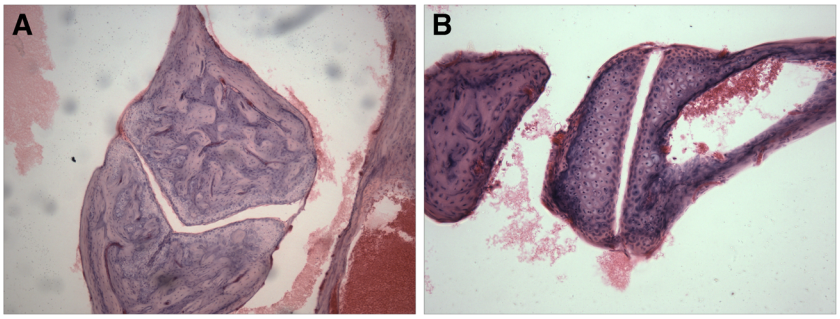

Fig. 4. Histology of ossicular joints in the gerbil middle ear, illustrating the presence of synovial gaps (courtesy of Clarinda Northrop). **A** Incudomallear joint. **B** Incudostapedial joint.

results of the simulations are compared with the experimental measurements in the frequency domain and, as in our experimental studies, we focus on the frequency range between 0.2 and 10 kHz.

Time Dependence An increase of 50 % in the time span of the simulation (from 50 to 75 ms) changed the responses by less than 0.03 dB, so the time span of 50 ms was used in order to reduce computation time. The selected time span provides a frequency resolution of 12 Hz. To study the effect of the time step on the responses, we ran simulations with time steps of 50, 30, 15, 10 and 5 μs. When the time step is fine enough, its effect on the responses becomes negligible. This range of time steps causes negligible effects for frequencies below 2 kHz. At 9 kHz, compared with the smallest time step (5 μs), the four larger time steps (from the largest to smallest) resulted in maximal magnitude changes in the umbo response of 30, 6, 2 and 0.8 nm/Pa and phase errors of 374, 73, 22 and 12°, respectively. As a trade-off between accuracy and length of computation time, we chose a time step of 10 μs for our simulations.

Mesh Dependence The original mesh that resulted from image segmentation, surface triangulation and volume mesh generation contained about 3300 triangular elements and 46200 tetrahedral elements. We used Code_Aster's Homard utility (Nicolas and Fouquet 2013) to refine the mesh by dividing each triangle into four coplanar triangles. This increased the number of triangular elements by a factor of four and the number of tetrahedral elements by a factor of eight. The refined mesh resulted in only a 0.2 dB increase in the umbo magnitude at the lowest frequency (200 Hz) and at the resonance. It caused a decrease of only 24 Hz in the resonance frequency, no difference in the break-up frequency of the pars tensa (to within our frequency resolution of 12 Hz), and no visible changes in the frequency-response shapes. Based on these results, we chose to perform this study with the original mesh.

Effect of Viewing Angle The simulations provide 3-D displacement vectors. Unless otherwise specified, all results from the model are presented in terms of the vector components parallel to the direction of the laser beam in our experiments (Maftoon et al. 2013, 2014). Panels b and c in Figure 1 show the range of viewing directions that we had in different experimental animals in those experiments. Because the viewing directions in most measurements were close to that of panel b, the model results in this paper are presented for this view. Changing the viewing angle to that of panel c, a change of about 20°, causes a difference of about 3 dB in the umbo response and less than 7 dB in the pars-tensa responses except at very sharp minima, and causes negligible changes in the frequencies of response features.

Baseline Material Properties

The experimental ranges of material properties from the literature and the values used in the baseline model are summarized in Table 1.

StiffnessDue to the small displacements occurring in the middle ear in response to the sound pressure, all materials in the model were assumed to be linearly elastic. All soft tissues were modelled as nearly incompressible, with a baseline Poisson's ratio of 0.49 (Funnell and Laszlo 1982).

*Pars Tensa*The stiffness of the pars tensa has large effects on middle-ear responses and a number of experimental studies have been dedicated to measuring it in different species, including one study in gerbil (Aernouts and Dirckx 2012). To justify the value that we have chosen for our simulations, we situate it with respect to values in the literature.

von Békésy (1960) estimated the bending stiffness of the pars tensa to be 20 MPa by applying a static force at the end of a cantilevered flap. Kirikae (1960) estimated a Young's modulus of 40 MPa by vibrating (at 890 Hz) a strip of pars tensa weighted at one end. Decraemer et al. (1980) and Cheng et al. (2007) estimated a Young's modulus of 23 and 22 MPa, respectively, at higher strains

Table 1 Range of experimental estimates of the material properties from the literature and the baseline values used in this study. Considerations and methods used are detailed in the text

	Range in literature	*Baseline*	*Comment*
Young's modulus of pars tensa (MPa)	2.1 (Aernouts et al. 2012) to 118 (Aernouts and Dirckx 2012)	10	Single-layer and isotropic
Young's modulus of pars flaccida (MPa)	0.42 (Agache et al. 1980) to 2 (Geerligs et al. 2011)	2	Human forearm and abdominal skin
Young's modulus of posterior incudal ligament (MPa)	None	10	Assumed equal to that of the pars tensa
Young's modulus of stapedial annular ligament (kPa)	10 (Lynch et al. 1982)	10	
Young's modulus of incudomallear and incudostapedial joints (MPa)	0.27 (Zhang and Gan 2011)	0.27	Calculated based on their incudostapedial measurements
Young's modulus of ossicles	16±3 (Soons et al. 2010)	16	Measured for incus and malleus
Soft tissue density (kg/m^3)	1000 to 1200 (Funnell and Laszlo 1982)	1100	Between densities of water and undehydrated collagen
Mass of malleus (mg)	1.145 (Nummela 1995)	1.145	Measured average value
Mass of incus (mg)	0.633 (Nummela 1995)	0.633	Measured average value
Mass of stapes (mg)	0.116 (Nummela 1995)	0.116	Measured average value

from uniaxial tensile testing of human pars-tensa strips. Gaihede et al. (2007) applied static pressure in the ear canal in vivo and measured volume changes due to TM deformation. To calculate the Young's modulus they assumed that the TM is a flat circular membrane; this simplistic model resulted in Young's modulus estimates of 10.3 and 6.9 MPa for their young and old human subjects, respectively. Huang et al. (2008) performed static indentation measurements on small human pars-tensa samples and used FE modelling to obtain the Young's modulus after relaxation. They calculated values of 17.4 to 19.0 MPa (in-plane) and 0.6 MPa (through-thickness). Daphalapurkar et al. (2009) removed the epidermal layer[7] of the pars tensa and then applied the same approach as Huang et al. They calculated higher values of the Young's modulus: 25.7 to 37.8 MPa (in-plane) and 2 to 15 MPa (through-thickness). It is not clear why the through-thickness Young's modulus of the pars tensa is so different in these two studies. Luo et al. (2009), doing uniaxial tensile testing on pars-tensa strips, obtained Young's moduli of 45.2 to 58.9 MPa for the radial direction and 34.1 to 56.8 MPa for the circumferential direction at strain rates of 300 to 2000 s^{-1}. Aernouts et al. (2010, 2012) and Aernouts and Dirckx (2012) used in situ indentation measurements and fitting with an isotropic single-layer FE model to obtain Young's moduli of the pars tensa in the rabbit, human and gerbil. Aernouts et al. (2010) obtained quasi-static Young's moduli of 30.4 MPa for the rabbit pars tensa if the Poisson's ratio in the model was 0.3 to 0.4 and 26.4 MPa if the material was considered to be nearly incompressible (Poisson's ratio near 0.5). Aernouts et al. (2012) obtained values of 2.1 to 4.4 MPa at 0.2 Hz for the human pars tensa. Aernouts and Dirckx (2012) estimated the Young's modulus to be between 71 and 106 MPa at 0.2 Hz and between 79 and 118 MPa at 8.2 Hz for the gerbil pars tensa. Their results for rabbit were comparable to those from other groups but their values were high for gerbil and low for human. Hesabgar et al. (2010) performed in situ indentation measurements and Ghadarghadar et al. (2013) performed in situ pressurization measurements, in both cases on the rat pars tensa. Single-layer FE model fitting was used in both studies to estimate the Young's modulus, resulting in values of 21.7 and 22.8 MPa, respectively. These values do not seem to be consistent with the suggestion by Aernouts et al. (2012) that the discrepancy between their gerbil and human Young's modulus values were due to "better high-frequency hearing of gerbil", since the rat also has good high-frequency hearing.

Some authors have used orthotropic models for the pars tensa and assigned different Young's moduli in the radial and circumferential directions (e.g., Sun et al. 2002). Some studies have used hyperelastic (e.g., Aernouts et al. 2010) or visco-hyperelastic (Motallebzadeh et al. 2013) constitutive equations for the pars tensa.

All of the above studies considered the pars tensa as a single layer of homogeneous material. Rabbitt and Holmes (1986) used an asymptotic analytical analysis and modelled the pars tensa as a ground substance and two sets of locally orthogonal fibres. They concluded that the pars tensa has strong anisotropy dictated by the local density of fibres and that the Young's modulus may vary by over one order of magnitude from one point to another. Fay et al. (2005) considered the multilayer nature of the pars tensa in estimating its Young's modulus. In the human, they estimated the Young's modulus to be from 100 to 300 MPa. In the cat, they

[0] Note that their Figure 3, also used by Volandri et al. (2011), neglects the subepidermal and submucosal connective-tissue layers that lie lateral and medial to the radial and circular fibre layers (Lim 1970).

reported a wider range, 30 to 400 MPa. The fact that their estimates are high is to be expected since they apply to the thickness of just the fibrous layers of the TM. Later, Fay et al. (2006) used Young moduli of 100 and 80 MPa for the radial and circumferential fibre layers, respectively. Tuck-Lee et al. (2008) used a high Young's modulus (100 MPa) for both the radial and circumferential fibres and a low Young's modulus (1 MPa) for the ground substance in a multilayer model.

As seen above, estimates for the Young's modulus of the pars tensa have been very diverse (see a summary by Volandri et al. 2011).[8] In most linearly elastic isotropic models, however, Young's moduli of 20 to 40 MPa were used. For simplicity, and because the quantitative distribution of the layer thicknesses and the difference between the radial and circumferential Young's moduli are not well known, we modelled the pars tensa as a single layer of isotropic material. Chole and Kodama (1989) reported that the collagen fibres are less dense in gerbil than in human and in this study we chose a Young's modulus of 10 MPa for the pars tensa. It is much lower than the values reported by Aernouts and Dirckx (2012) for the gerbil but it is within of the range of the measured values that have been reported for other species, and with this value the model gives results that are within the range of our experimental data collected in gerbils in vivo (Maftoon et al. 2014). The choice of this parameter will be discussed again later.

*Pars Flaccida*The pars flaccida is a continuation of the external ear canal skin (Lim 1968b) that spans Rivinus' incisure. Agache et al. (1980) estimated the Young's modulus of the human forearm skin in vivo to be 0.42 MPa in their younger subjects and 0.85 MPa in subjects more than 30 years old. Recently, Geerligs et al. (2011) estimated the Young's moduli of the human epidermis and *stratum corneum* to be between 1 and 2 MPa using in vitro indentation measurements on abdominal skin.

At a low frequency (200 Hz) we measured a displacement magnitude of 1.5 μm/Pa (Maftoon et al. 2014, gerbil E) near the centre of the pars flaccida. Assuming that the pars flaccida is a circular disk subjected to a uniform static pressure (Timoshenko and Woinowsky-Krieger 1959, p. 57, Eq. 68) with a radius of 0.7 mm and a constant thickness of 23.5 μm, with a Poisson's ratio of 0.49 and simply supported all around its periphery, then a centre deformation of 1.5 μm/Pa leads to a Young's modulus of 6.4 MPa. If the circular disk is considered to be fully clamped all around its periphery, a Young's modulus of 1.7 MPa is obtained (ibid, p. 55, Eq. e). Gea et al. (2009) demonstrated that the boundary of the pars flaccida can be considered to be simply supported at the bony edge but it is neither simply supported nor fully clamped at its interface with the pars tensa.

Based on the Young's modulus measurements on the skin and on the simplistic analysis of a circular plate, we assumed a Young's modulus of 2 MPa, a round number with which the model gives results that are in the range of experimental data, as seen in the "Results" section. We have experimentally observed that, with a widely opened middle-ear cavity, the pars-flaccida effect on other responses is limited to a narrow frequency range and is very shallow (Maftoon et al. 2014). Consistent with this, in our open-cavity simulations, the pars flaccida is an almost independent structure whose parameters have little effect on the responses of the rest of the system.

*Other Structures*Fumagalli (1949) reported that the posterior incudal ligament is composed of highly organized collagen fibres in various species. In the absence of experimental data, we assumed that the Young's modulus of the ligament is equal to that of the pars tensa, which is partly composed of highly organized collagen fibres.

We assumed the Young's modulus of the stapedial annular ligament to be 10 kPa, as estimated by Lynch et al. (1982) in the cat. A recent measurement by Gan et al. (2011) in human temporal bones reported a shear modulus of 3.6 kPa for the smallest measured shear stress. Using this value and assuming an incompressible material, the Young's modulus of the stapedial annular ligament would be 10.8 kPa, close to the value estimated by Lynch et al.

Zhang and Gan (2011) performed uniaxial tension and compression tests on the human incudostapedial joint in the piston direction of the stapes. Fitting a straight line to the portion of their average experimental tension curve with displacements below 0.03 mm (in their Fig. 4B), and using dimensions given by them (length L and mean length a and width b), we calculated a Young's modulus of 0.27 MPa. We used this value in our model for the Young's moduli of both incudomallear and incudostapedial joints.

The ossicles were modelled with a Poisson's ratio of 0.3 (Elkhouri et al. 2006). Recently, Soons et al. (2010) reported a Young's modulus of 16±3 GPa for the rabbit incus and malleus. We used their average value (16 GPa) for the Young's moduli of all three ossicles.

[8] The very high value of 20 GPa reported in Table 3 of Volandri et al. (2011) was a typographical error (GPa rather than MPa) in the original paper by Gentil et al. (2005) (personal communication with Gentil). The very low value of 1.5 MPa used by Lesser and Williams (1988) was for a 2-D model. The very low values used by Funnell and Laszlo (1978) and Funnell (2001) for Ec were intended to be extreme examples of anisotropy, not realistic estimates. The very low values used by Ferrazzini (2003) were for a pars-tensa model that was overly thick and was not smooth.

MassFor all soft tissues, a density of 1100 kg/m^3 was chosen as being in the middle of the possible range between the density of water (1000 kg/m^3) and that of undehydrated collagen (1200 kg/m^3) (Funnell and Laszlo 1982).

Sim et al. (2007) reported mean density values for the malleus and incus in human temporal bones as 2390 and 2150 kg/m^3, respectively. Cohen et al. (1992) reported masses for the malleus and incus in gerbils. Nummela (1995) provided the masses for the malleus and incus, close to the ones reported by Cohen et al., and also the mass of the stapes. Using volumes from their 3-D models of the gerbil ossicles, and mass values from Nummela (1995), Buytaert et al. (2011) reported average densities of 1740 kg/m^3 for the malleus and incus and 1370 kg/m^3 for the stapes. In the present work, based on volumes calculated from our model and the mass data reported by Nummela (1995), we calculated densities of 1918, 1855 and 1565 kg/m^3 for the malleus, incus and stapes, respectively.

DampingRayleigh damping was used for all model components. The Rayleigh damping matrix is given by α **M**+β **K**, where **M** is the mass matrix and **K** is the stiffness matrix. The damping parameters α and β are the least well-known parameters of the middle ear. We assumed a stiffness-proportional damping (i.e., α=0) for all middle-ear structures and divided the soft tissues into ones with highly organized collagen fibres (the pars tensa (Lim 1968a) and posterior incudal ligament (Fumagalli 1949)) and ones with abundant elastic fibres (the pars flaccida (Lim 1968b) and the stapedial annular ligament, incudomallear joint and incudostapedial joint (e.g., Davies 1948; Harty 1953)). In a series of simulations we varied the damping parameters, with the other material properties fixed at their baseline values, and compared model results with responses that we measured in gerbil ears in terms of the magnitude of the umbo response at low frequencies (well below the middle-ear resonance) and at the resonance peak, the break-up frequency, and the bandwidth of the high-frequency (above break-up frequency) features in the pars-tensa responses. Based on these comparisons, we used a damping parameter β of 2×10^{-6} s for the structures with highly organized collagen fibres and 3×10^{-5} s for the structures with abundant elastic fibres. We assumed that the ossicles have a damping parameter of 2×10^{-7} s, one order of magnitude less than that of the pars tensa. In the "Results" section, we explore how changing the damping parameters of each structure affects the responses.

Cochlear Loadde La Rochefoucauld et al. (2008) and Ravicz et al. (2008) measured the cochlear input impedance in gerbil and concluded that it is resistive with a "roughly" constant magnitude below 30 kHz. Following their conclusions, we used an average cochlear input impedance of 4×10^{10} Pa s/m (de La Rochefoucauld et al. 2008, Fig. 9). They used a stapes footplate area of 0.62 mm^2. From these values, we calculated a viscous damping coefficient of 15.4×10^{-3} N s/m. In our simulations, we uniformly distributed this damping to the four dashpots attached to the stapes footplate parallel to the piston-motion direction (two at the ends of the long axis and two at the ends of the short axis) to represent the cochlear load.

Sensitivity Analysis

After establishing the baseline model using the material properties specified in the "Baseline Material Properties" section, we performed a one-variable-at-a-time sensitivity analysis. We increased and decreased each material parameter by 10 % of its baseline value while keeping all other parameters at their baseline values. For all stable isotropic elastic materials, the Poisson's ratio has a finite range, from –1 for completely compressible materials to 0.5 for completely incompressible materials (e.g., Wang and Lakes 2005; Greaves et al. 2011). This is in contrast with the Young's modulus, density and thickness, which in principle can range from zero to infinity. To avoid difficulties that arise when Poisson's ratio is varied by ±10 % near its upper limit of 0.5, for the purposes of the sensitivity analysis we defined material stiffness in terms of the Young's modulus (E) and the bulk modulus (B) instead of the Young's modulus and Poisson's ratio (v), based on the relationship

$$B = \frac{E}{3(1-2v)}. \quad (1)$$

Adjusted Material Properties

As will be seen in the "Results" section, although the baseline material properties ("Baseline Material Properties" section) result in responses that are very similar to experimental results, in some respects they fall on the high side of or outside the experimental ranges. We have therefore used the results of our sensitivity analysis to obtain a preliminary adjusted parameter set. In order to do so, we changed the sensitive parameters of the baseline model one at a time, in 10 % steps, in the direction that the sensitivity analysis suggested. In the adjusted parameter set, the Young's modulus of the pars tensa was increased by 20 %; the density of the TM was set to 1200 kg/m^3, at the physiological upper limit described in the "Mass" section; and the thickness of the TM was considered to be 20 % larger than the average thickness data of Kuypers et al. (2005). The densities of the ossicles

were considered to be 20 % larger than the baseline values, which can be thought of as reflecting a small increase in the sizes of the ossicles. The Young's moduli of the incudomallear and incudostapedial joints were set to two times the baseline value. The cochlear input impedance was taken to be 6×10^{10} Pa s/m, near the upper end of the experimental data of de La Rochefoucauld et al. (2008).

RESULTS

Umbo and Pars-Flaccida Responses

In our experimental measurements (Maftoon et al. 2013, 2014) and in earlier studies (e.g., Lee and Rosowski 2001; Rosowski and Lee 2002), it was observed that the vibrations of the pars flaccida affect responses measured at the umbo. In this section, we present these responses together. Recall that for all experimental results from Maftoon et al. (2014) the estimated ideal open-cavity frequency responses are shown.

Low Frequencies. Figure 5 shows the estimated ideal open-cavity umbo responses in nine experimental ears from Maftoon et al. (2014), as well as the umbo responses from the model with the baseline parameter set and from a model with the adjusted parameter set described in the "Adjusted Material Properties" section. The magnitude of the experimental umbo responses at the lowest frequency was between 110 and 330 nm/Pa, compared with 260 and 200 nm/Pa for the baseline and adjusted models, respectively. The baseline model response is on the high side of the variability seen in the experimental responses. Similar to the experimental responses, the umbo in the model moves with a phase of zero at the lowest frequency.

Figure 6 shows simulated responses at the centre of the pars flaccida, as well as the response at the umbo (the same curve as shown in Fig. 5). In our experimental measurements in gerbil ears, we often observed that the pars flaccida is retracted into the middle-ear cavity. Figure 6 shows the experimental open-cavity pars-flaccida responses for ear E from Maftoon et al. (2014), the only ear in which we could measure the response of a naturally flat pars flaccida, as well as the one ear from Rosowski et al. (1997). At the lowest frequency, the centre of the pars flaccida in the model has a phase of zero and a magnitude of 2.2 μm/Pa. The experimental ears show phases of nearly zero and magnitudes of 1.5 μm/Pa (Maftoon et al.) and 2.5 μm/Pa (Rosowski et al.) at low frequencies.

Similar to experimental observations (Maftoon et al. 2013, Fig. 3), the umbo and pars flaccida of the model move almost in phase with each other up to about 700 Hz, as seen in Figure 6. The model pars flaccida shows a resonance at about 820 Hz. Between about 700 and 950 Hz, the umbo response from the model shows a feature that includes a shallow maximum (at 780 Hz) followed by a shallow minimum (at 880 Hz) in the magnitude, and a local minimum (at 840 Hz) in the phase. The correspondence of this feature in the umbo response to the resonance of the pars flaccida was discussed in Maftoon et al. (2013). In Figure 5 only ears E and K had a naturally flat pars flaccida; in all the other ears the pars flaccida was

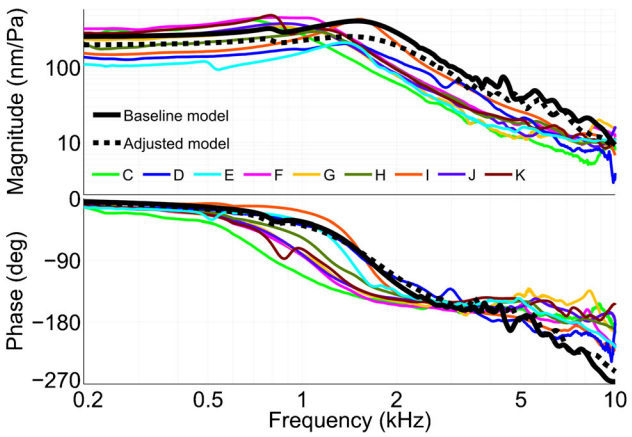

Fig. 5. Simulated umbo responses (*black lines*), and responses from experimental measurements in 9 gerbil ears with partial openings in the cavity wall (*coloured lines*). The gerbils (*C to K*) were those reported by Maftoon et al. (2014) and the method proposed in that paper was used here to estimate the ideal open-cavity responses; that is, although the responses were measured with a partial opening in the middle-ear cavity wall, they have been adjusted so they appear as though they were measured with no cavity wall. The simulated responses are shown for baseline parameters (*solid line*) and adjusted parameters (*dashed line*), as discussed in the text.

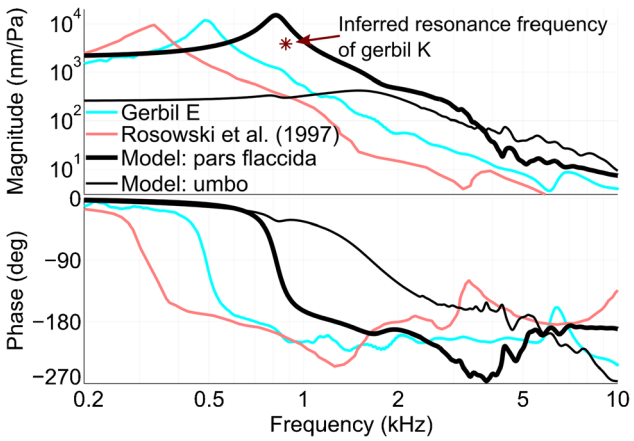

Fig. 6. Simulated and experimental pars-flaccida responses and a simulated umbo response. *Thick black* simulated pars-flaccida response. *Thin black* simulated umbo response. *Pink* experimental pars-flaccida response in a gerbil ear reported by Rosowski et al. (1997). *Cyan* experimental pars-flaccida response in the ear of gerbil E of Maftoon et al. (2014). *Asterisk* frequency of the pars-flaccida resonance inferred from the umbo response in gerbil K of Maftoon et al. (2014).

retracted into the middle-ear cavity. The umbo responses in these two ears show the pars-flaccida feature in both magnitude and phase. The shallow maximum and shallow minimum are 60 and 135 Hz apart and the ratios of their magnitudes are 1.3 and 1.8 in gerbils E and K, respectively. The shallow maximum and shallow minimum in the model umbo result are 100 Hz apart and the ratio of their magnitudes is 1.1.

The magnitude of the simulated response at the centre of the pars flaccida at resonance (800 Hz) is 15 μm/Pa. The pars-flaccida responses in the two experimental ears (Fig. 6) show resonances at 350 and 500 Hz with magnitudes of 9.5 and 11.6 μm/Pa. We were not able to record the pars-flaccida response in gerbil K but the resonance frequency of the pars flaccida inferred from the umbo response is at about 900 Hz as indicated in Figure 6 by an asterisk. The simulated response matches the inferred peak frequency for gerbil K quite well. The pars-flaccida response in the model shows a full width at half maximum of 210 Hz. This value (a measure of damping) was observed to be between 110 and 230 Hz in the experimental measurements.

The possible causes of the retraction of the pars flaccida into the middle-ear cavity were discussed by Maftoon et al. (2013). To replicate this experimental condition in the model, we applied a static pressure of 100 Pa to the lateral side of the pars flaccida. This pressure had no physical significance; rather, it was just a numerical trick to produce a geometry of the retracted pars flaccida that was similar to what we observed in our experiments. As Figure 7A shows, this static pressured deformed the original flat pars flaccida to an inverted dome-like shape like what we observed experimentally. Figure 7B shows that retraction of the pars flaccida removes the pars-flaccida feature from both magnitude and phase of the simulated umbo response.

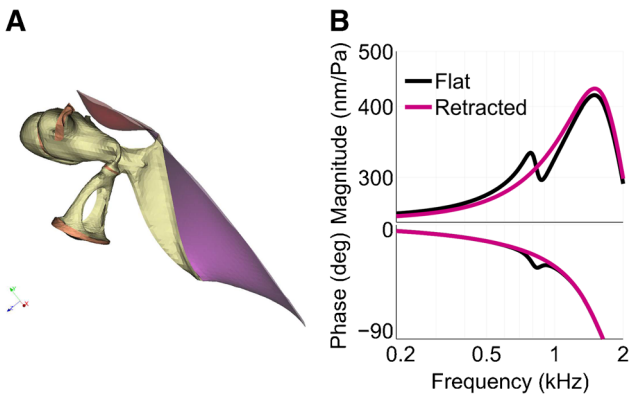

Fig. 7. **A** 3-D model of gerbil middle ear with retracted pars flaccida. **B** Simulated umbo responses with flat and retracted pars flaccida. In our experimental measurements in gerbil ears we often observed that the pars flaccida is retracted into the middle-ear cavity. To replicate this experimental condition in the model, we applied a static pressure of 100 Pa to the lateral side of the pars flaccida.

Mid- and High Frequencies. Similar to experimental observations (e.g., Fig. 3 of Maftoon et al. 2013), the displacement magnitude at the centre of the pars flaccida remains higher than that of the umbo up to about 3.5 kHz (Fig. 6). At higher frequencies, we observed experimentally that the pars-flaccida magnitude was at the level of or as much as 7.5 dB lower than that of the umbo. A similar pattern is observed in the model result, with the pars-flaccida magnitude going to as much as 10 dB below that of the umbo.

The simulated baseline and adjusted umbo responses in Figure 5 show rather broad resonances with peaks of 420 and 260 nm/Pa at 1.5 kHz, respectively. In the umbo responses of all experimental ears in Figure 5, the resonance frequencies are between 940 Hz and 1.6 kHz and the magnitudes at the resonance are between 210 and 460 nm/Pa. The frequency and magnitude at the resonance peak from the baseline model are on the high side of the experimental results. The ratio of the umbo magnitude at the resonance to that at low frequencies is between 1.2 and 2.9 in these experimental ears, compared with 1.6 and 1.3 for the baseline and adjusted models, respectively.

In experimental ideal open-cavity responses, the width of the resonance (in terms of the full width at half maximum of the umbo velocity response) is between 1.0 and 2.2 kHz. This quantity is 1.8 kHz in the model response. As for the experimental ears, the umbo response for the model shows a roll-off with substantial irregularities. For both measurements and model, the irregularities have bandwidths of a few hundred hertz, magnitude changes of a few decibels, and phase changes of a few tens of degrees. For frequencies above the resonance frequency, the simulated umbo response is higher than any of the measured responses.

Manubrial Response

Figure 8 shows the baseline model responses at five points along the manubrium. Similar to experimental observations (Maftoon et al. 2014, Fig. 18), the magnitude increases from the lateral process to the umbo, and all points along the manubrium move in phase with one another up to about 4.5 kHz, except in a narrow range (50 Hz) at about 3.3 kHz (not visible in Fig. 8). This pattern in the responses is consistent with a classical rotation of the malleus around a fixed axis of rotation at low frequencies. At the resonance peak, the umbo-to-lateral-process displacement magnitude ratio is 1.40, somewhat smaller than the ratios of 1.47 to 2.00 measured experimentally in the open-

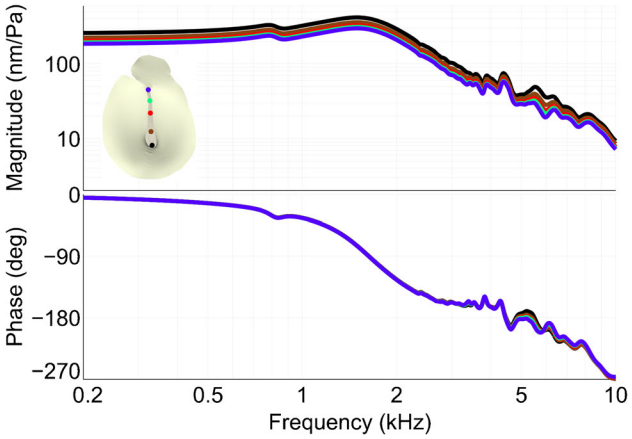

Fig. 8. Model responses at five locations along the manubrium. Between about 4.5 and 8 kHz, the phases show differences of more than 5°, with a maximum difference of 13° between the umbo and the lateral process at 5.4 kHz.

cavity condition. If the motions are calculated based on the view shown in Figure 1C instead of the one in Figure 1B, the umbo-to-lateral-process displacement magnitude ratio will be 1.90, close to the upper limit of the experimental observations.

In Figure 8 between about 4.5 and 8 kHz, the phases show differences of more than 5°, with a maximum difference of 13° between the umbo and the lateral process at 5.4 kHz. Above 7 kHz the manubrial points again move in phase with each other (within 5°). Experimentally, phase differences were seen above about 5 kHz.

Figure 9 shows the simulated displacements of the five manubrial points for four frequencies and for seven equally spaced time instants within each cycle. The locations of the points on the abscissa were determined by projection onto a plane perpendicular to the laser beam. The asterisk in each panel indicates the position of the anatomical axis of rotation, which was assumed to run from the anterior bony attachment of the malleus to the posterior tip of the short process of the incus. At the lowest frequency (200 Hz) the manubrium rotates as a rigid body around a fixed axis of rotation shown by the intersection of the instantaneous lines. This intersection is not exactly at our estimated anatomical axis of rotation but it is close to it. At the resonance peak (1.5 kHz), the manubrium again rotates as a rigid body around an almost fixed axis of rotation, at about the same position as before. The position of the axis of rotation starts to shift at frequencies above 1.8 kHz. At 5.4 and 9.5 kHz, the mode of vibration of the manubrium has clearly changed, with the position of the instantaneous axis of rotation moving throughout the cycle. At 5.4 and 9.5 kHz, the lines show slight deflections that might be due to mild bending of the manubrium. Changes in the position of the axis and indications

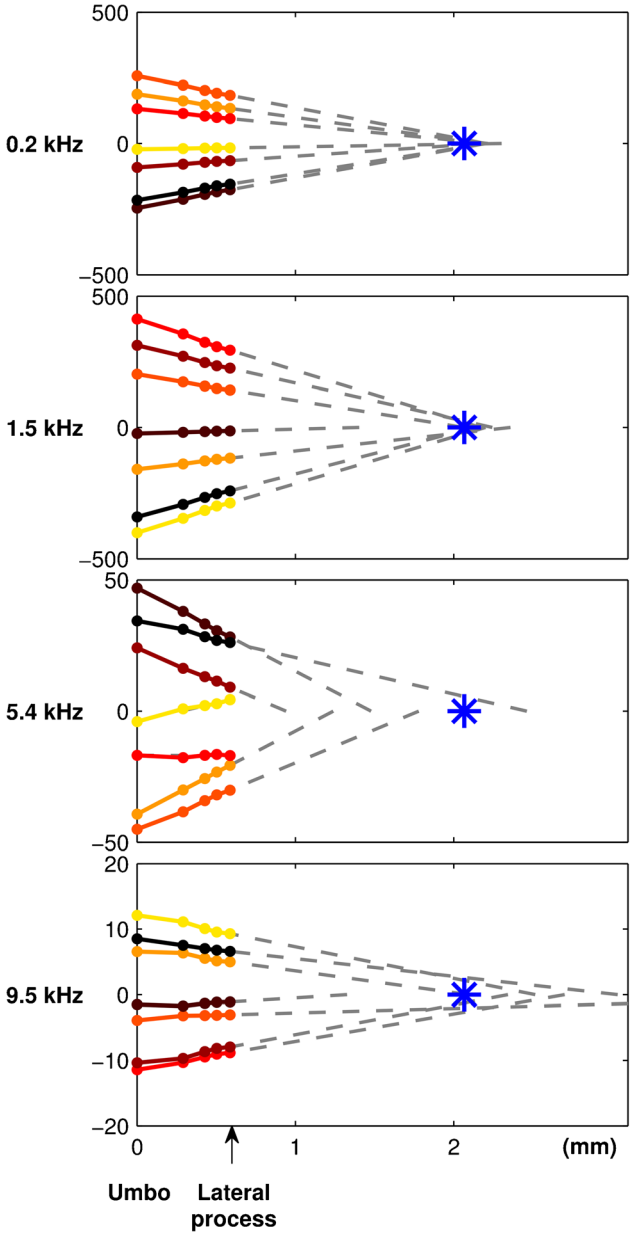

Fig. 9. The displacements of five points along the manubrium at four frequencies and for seven equally spaced time instants within each cycle. The locations of the points on the line were determined by projection onto a plane perpendicular to the laser beam. We assumed that the anatomical axis of rotation (the position where the axis crosses the figure plane is indicated by an *asterisk*) runs from the anterior bony attachment of the malleus to the posterior tip of the short process of the incus. At the two higher frequencies, the axis of rotation is not fixed and the *lines* suggest slight bending of the lower half of the manubrium.

of possible manubrial bending were also seen experimentally (Maftoon et al. 2013, Fig. 6).

Pars-Tensa Response

Figure 10 shows baseline model responses for six pars-tensa points and one manubrial point at the level of

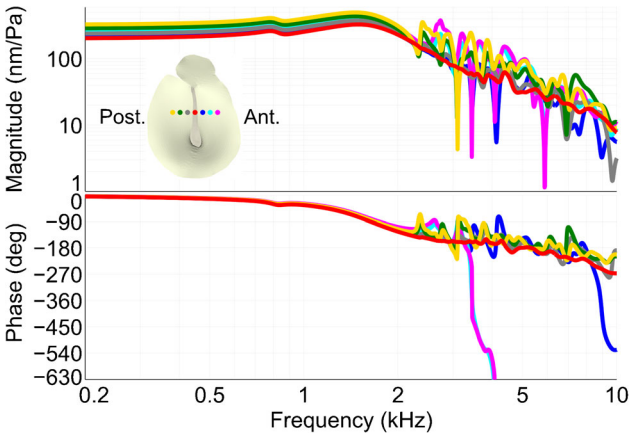

Fig. 10. Model responses of six pars-tensa points and one manubrial point at the level of the middle of the manubrium. For frequencies above 2 kHz the responses of the pars tensa are much less smooth than that of the manubrium.

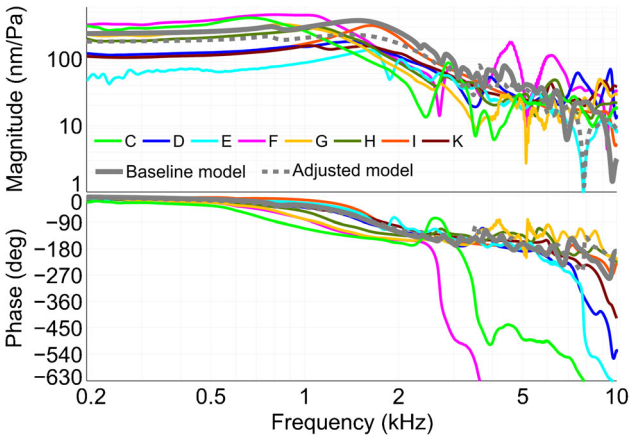

Fig. 11. Simulated pars-tensa response (*grey*) at a point posterior to the manubrium at the level of the middle of the manubrium (the *grey point* in the schematic inset in Fig. 10), together with responses from measurements in eight gerbil ears (with partial openings in the cavity wall) at the first bead posterior to the manubrium at the level of the middle of the manubrium (Maftoon et al. 2014). As in Figure 5, the experimental responses in this figure are estimated ideal open-cavity responses.

the middle of the manubrium. All points vibrate in phase for frequencies up to about 2 kHz. At these frequencies, the pars-tensa points exhibit a simple motion pattern. Similar to manubrial points, all pars-tensa responses show the pars-flaccida feature. At low frequencies, the magnitude at the manubrium is the smallest and, for the same distances from the manubrium, points on the posterior side show larger displacements than the ones on the anterior side. The displacement pattern at low frequencies is similar to the patterns observed in gerbil ears experimentally (Maftoon et al. 2013, Fig. 9).

At higher frequencies, the simple in-phase motion breaks up and each point shows different frequency-dependent magnitudes and phases. The break-up frequency for the model is 2 kHz, which is within the range of 1.8 to 2.8 kHz observed experimentally.

The experimental inter-animal variability of the pars-tensa motion is illustrated in Figure 11. The pars-tensa responses are more different from ear to ear than the manubrial responses are. The variability in this figure is presumably due not only to differences among animals but also to slight differences in the locations of the measurement points, because of the complexity of the spatial vibration patterns. Large differences at specific frequencies are only seen when comparing pars-tensa responses above the break-up frequency, when a peak in one ear occurs at the same frequency as a trough in another ear. The umbo responses presented in Figure 5 show significantly less variability, the amplitude ratios differing by factors of less than 4 at each specific frequency. The smoother, spatially integrated umbo response is more directly related to what is finally transferred to the cochlea. This figure includes the estimated ideal open-cavity responses on the pars tensa about 150 μm posterior to the manubrium in eight experimental ears. The results from the model with the baseline and adjusted parameter sets at a similar location are also plotted (in grey) in this figure. The curves show complex responses which are all different from one another. Similar to what is seen in Figure 5, the resonance frequency and the magnitude response from the baseline model is on the high side of the range seen in the experimental responses. Similar to the experimental responses, the pars-tensa responses from the model show features with frequency bandwidths of a few hundred to a few thousand hertz. The simulated responses in Figure 10 show about as much fine structure as do the measured responses in Figure 11. The particular simulated node shown in Figure 11 has less-sharp features, but so do some of the experimental results shown in the same figure. As in the experimental responses in Figure 11, the phases of some points in the model results in Figure 10 show very large phase shifts at some sharp magnitude minima.

Stapes Response

The ratio of umbo displacement to stapes displacement is often specified in terms of a lever ratio (although Fig. 9 shows that the lever model with a fixed fulcrum does not hold for frequencies above a few kHz). In order to calculate this ratio in our model, we assumed the anatomical axis to be as described in the "Manubrial Response" section. The lengths of the 3-D lines drawn perpendicular to the anatomical axis from the end point of the central line of the long process of the incus and from the umbo are 1.0 and 3.2 mm, providing a lever ratio of 3.2. Using 2-D

calculations, Rosowski et al. (1999) calculated the average anatomical lever ratio in seven gerbil ears to be 3.1, and using their vibration measurements they estimated a lever ratio of 3.5 at low frequencies. The ratio of umbo displacement to stapes displacement in the gerbil measurements of Decraemer et al. (2014) was between 3 and 4 at low frequencies.

Figure 12 shows the displacement of the centre of the stapes footplate in the direction of piston-like motion (solid black line). (The piston-like direction was taken as the direction normal to the plane passing through the anatomical axis of rotation and the end point of the central line of the long process of the incus.) Dividing the umbo displacement, in the direction of the normal to the plane passing through the anatomical axis of rotation and the umbo, by the piston-like stapes displacement gives a lever ratio of 3.2 at the lowest frequencies with both baseline and adjusted parameter sets. Above 500 Hz, the lever ratio starts to decrease with frequency, going down to 2.3 (−30 %) at about 5 kHz. Above this frequency, the lever ratio shows drastic changes with frequency.

The stapes responses in Figure 12 show resonances at the same frequency (1.5 kHz) as the umbo responses in Figure 5. A similar correspondence between the resonance frequencies of the stapes and umbo responses was experimentally observed by Rosowski et al. (1999). The phase of the stapes response starts to depart from that of the umbo at frequencies as low as 300 Hz (where the difference is 2°). At 2 kHz, this phase difference becomes 15° and

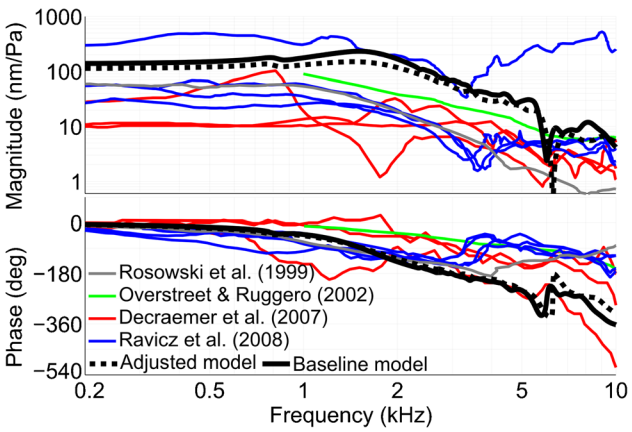

Fig. 12. Piston component of the stapes footplate displacement from the model (*solid black line*) and measured experimentally in gerbil ears. *Grey* the mean of six ears from Rosowski et al. (1999, Fig. 4); *green* the median of eight adult ears from Overstreet and Ruggero (2002, Fig. 2); *red* three ears from Decraemer et al. (2007, Figs. 6, 10 and 12); *blue* four ears from Ravicz et al. (2008, Fig. 4). Except for the responses from Decraemer et al., the experimental responses were originally presented in terms of velocities but for this figure we have converted them to displacements. The simulated umbo response (in the direction of the normal to the plane passing through the anatomical axis of rotation and the umbo) is also shown (*dashed black line*).

continues to grow with frequency except between 5.8 and 7.8 kHz.

Figure 12 also includes stapes displacement responses from four experimental studies in gerbil ears: the mean of six ears from Rosowski et al. (1999, Fig. 4), shown in grey; the median of eight adult ears from Overstreet and Ruggero (2002, Fig. 2), shown in green; three ears from Decraemer et al. (2007, Figs. 6, 10 and 12), shown in red; and four ears from Ravicz et al. (2008, Fig. 4), shown in blue. (Except for the responses from Decraemer et al., the experimental responses were originally presented in terms of velocities but for this figure we have converted them to displacements.) The experimental responses from Decraemer et al. (at about 6 kHz) and from Rosowski et al. and Ravicz et al. (between 3 and 4 kHz) are affected by the antiresonance due to the acoustic contribution of the hole in the middle-ear cavity wall (cf. Ravicz et al. 1992; Maftoon et al. 2014), an effect that of course is not present in the model results. The data of Overstreet and Ruggero do not show this effect, presumably because calculating the median of the responses filters out the effect. The stapes response from the model is on the high side of the variability seen in these experimental responses. The model manubrial and pars-tensa magnitude responses are also on the high side of our own experimental data, as indicated by Figures 6 and 11. The magnitude of the model response with adjusted parameters is slightly lower than the one from the baseline model.

The model stapes response shows minima in both magnitude and phase in the frequency range of 5.5 to 6.5 kHz. The dependence of this and other features on the middle-ear structures and model parameters will be explored in the next section.

Sensitivity Analysis

In this section, we present model results obtained as the model parameters are varied one at a time by ±10 % from their baseline values. In the figures presented in this section, response changes due to changes in the parameters of a particular model structure are consistently shown in the same colour (e.g., red for pars tensa), and each type of parameter is indicated by a unique symbol across all structures (e.g., circle for Young's modulus). These symbols are filled when the parameters are increased by 10 % and open when the parameters are decreased by 10 %.

Figure 13 shows the changes in the magnitude of the umbo response at a low frequency (200 Hz) as the parameters of the model were varied by ±10 %. For this amount of variation, the most influential parameters, in decreasing order of importance, are the thickness and Young's modulus of the pars tensa and the Young's moduli of the malleus and the stapedial

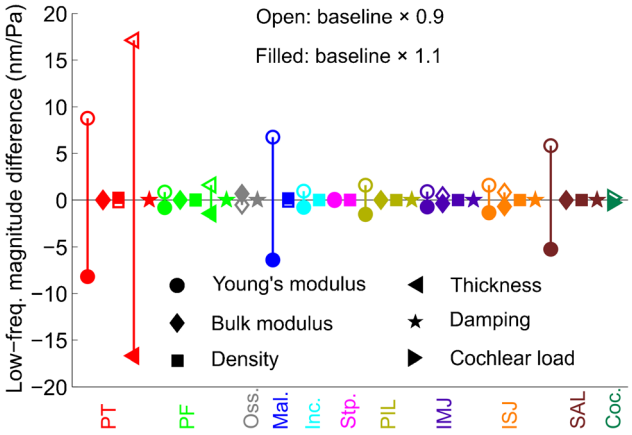

Fig. 13. Changes in the magnitude of the umbo response at a low frequency (200 Hz) as the parameters of the model were varied ±10 %. *PT* pars tensa, *PF* pars flaccida, *Oss.* ossicles, *Mal.* malleus, *Inc.* incus, *Stp.* stapes, *PIL* posterior incudal ligament, *IMJ* incudomallear joint, *ISJ* incudostapedial joint, *SAL* stapedial annular ligament, *Coc.* cochlear load. Changes due to the variation in parameters of each of these groups are shown in the *same colour*. Each parameter is shown by a *unique symbol* across all structures. The *symbols are filled* when the parameters were increased by 10 % and are *open* when the parameters were decreased by 10 %.

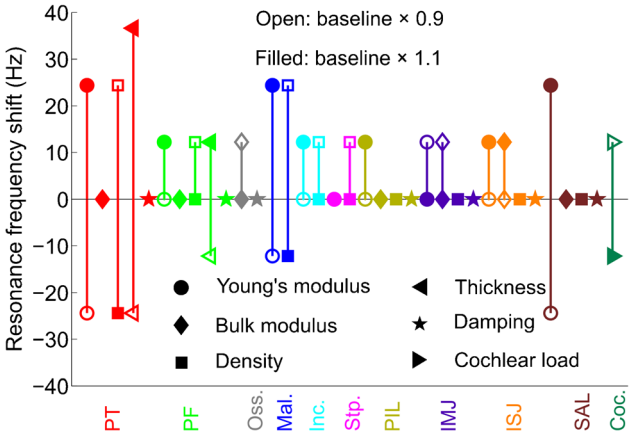

Fig. 14. Shifts in the middle-ear resonance frequency (seen in the umbo response) as the parameters of the model were varied ±10 %. *PT* pars tensa, *PF* pars flaccida, *Oss.* ossicles, *Mal.* malleus, *Inc.* incus, *Stp.* stapes, *PIL* posterior incudal ligament, *IMJ* incudomallear joint, *ISJ* incudostapedial joint, *SAL* stapedial annular ligament, *Coc.* cochlear load. Changes due to the variation in parameters of each of these groups are shown in the *same colour*. Each parameter is shown by a *unique symbol* across all structures. The *symbols are filled* when the parameters were increased by 10 % and are *open* when the parameters were decreased by 10 %. The frequency resolution in our analyses is 12 Hz.

annular ligament. All other parameters have effects of less than 3 nm/Pa (less than 1 dB).

As described in the "Umbo and Pars-Flaccida Responses" section, the umbo response shows a shallow maximum and a shallow minimum due to the pars flaccida. Variations in the thickness parameter cause the largest changes in these features. A 10 % decrease in the thickness shifted the maximum and minimum 50 and 60 Hz lower, respectively, and decreased their respective magnitudes by 5 and 10 nm/Pa. A 10 % increase in the thickness shifted both maximum and minimum 50 Hz higher and increased their respective magnitudes by 5 and 10 nm/Pa. The Young's modulus, density and damping of the pars flaccida are the next most influential parameters. As expected, increasing the Young's modulus or decreasing the density of the pars flaccida shifts the feature to higher frequencies, and increasing the pars-flaccida damping decreases the magnitude difference between the two extrema. Other parameters do not change the frequencies of the extrema.

Figure 14 shows the shifts in the middle-ear resonance frequency (as seen in the umbo response) due to parameter variations. Since the frequency resolution of our analyses is 12 Hz, the frequency shifts that are given are multiples of this number and changes smaller than that are not captured. Increasing and decreasing the thickness of the pars tensa cause frequency shifts of +36 and −24 Hz, respectively. Such an asymmetry is seen for other parameters as well (e.g., the Young's modulus and density of the malleus). The Young's moduli and densities of the pars tensa and the malleus and the Young's modulus of the stapedial annular ligament cause resonance-frequency shifts of up to 24 Hz. As expected, the Young's modulus and density of the pars tensa affect the resonance frequency oppositely, as do those of the malleus. Other parameters have effects of 12 Hz or less.

Effects of parameter variations on the magnitude of the umbo response at the resonance peak are shown in Figure 15. Increasing and decreasing the cochlear load cause changes of −35 and 42 nm/Pa (−0.7 and 0.8 dB), respectively. Other influential parameters, in decreasing order of importance, are the density, Young's modulus and thickness of the pars tensa, and the density and Young's modulus of the malleus. All other parameters have effects of less than 0.1 dB.

The effects of parameter variations on the low-frequency magnitude, resonance frequency and magnitude at the resonance peak of the pars-tensa response are similar to their effects on those features of the umbo response. As Figure 16 shows, the break-up frequency of the pars tensa is shifted by −124, −108, +48 and +36 Hz when the thickness and Young's modulus of the pars tensa, the cochlear load and the density of the pars tensa are decreased, respectively. Increasing these parameters causes opposite effects that are similar but not always the same in size. All other parameters have considerably less effect (less than 24 Hz) on the break-up frequency shift. Above the break-up, the high-frequency features in the pars-

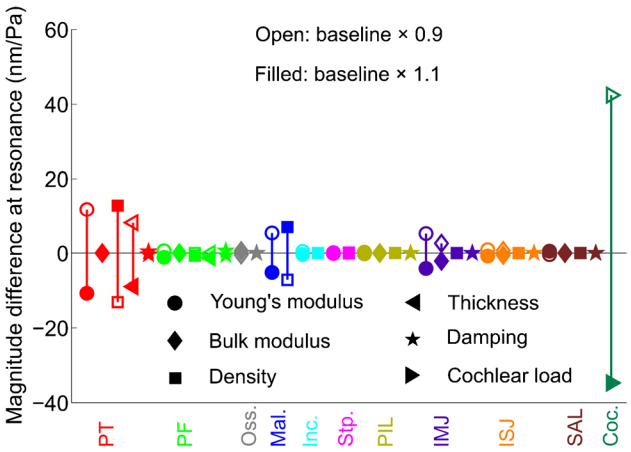

Fig. 15. Changes in the magnitude of the umbo response at the resonance peak as the parameters of the model were varied ±10 %. *PT* pars tensa, *PF* pars flaccida, *Oss.* ossicles, *Mal.* malleus, *Inc.* incus, *Stp.* stapes, *PIL* posterior incudal ligament, *IMJ* incudomallear joint, *ISJ* incudostapedial joint, *SAL* stapedial annular ligament, *Coc.* cochlear load. Changes due to the variation in parameters of each of these groups are shown in the *same colour*. Each parameter is shown by a *unique symbol* across all structures. The *symbols are filled* when the parameters were increased by 10 % and are *open* when the parameters were decreased by 10 %.

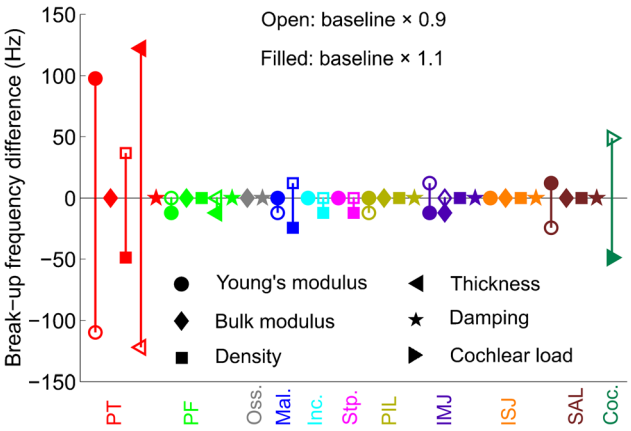

Fig. 16. Changes in the pars-tensa break-up frequency as the parameters of the model were varied ±10 %. *PT* pars tensa, *PF* pars flaccida, *Oss.* ossicles, *Mal.* malleus, *Inc.* incus, *Stp.* stapes, *PIL* posterior incudal ligament, *IMJ* incudomallear joint, *ISJ* incudostapedial joint, *SAL* stapedial annular ligament, *Coc.* cochlear load. Changes due to the variation in parameters of each of these groups are shown in the *same colour*. Each parameter is shown by a *unique symbol* across all structures. The *symbols are filled* when the parameters were increased by 10 % and are *open* when the parameters were decreased by 10 %.

tensa responses are most strongly influenced by the thickness, Young's modulus and density of the pars tensa and the damping of the pars tensa, in decreasing order of importance.

The low-frequency lever ratio changes less than 1 % for 10 % variations in all model parameters.

As mentioned above, the magnitude of the stapes response in Figure 11 shows a minimum between 5.5 and 6.5 kHz. We have explored the effects of parameters on the shape of this feature. Among all parameters, a 10 % decrease in the Young's modulus of the pars tensa causes the greatest change (an increase of 5 nm/Pa, about 1 dB) in the depth of the feature. The other parameters do not affect the depth of this feature much.

DISCUSSION

Study Approach

Baseline Model. One frequent criticism of finite-element models is that the many parameters that they have enable them to fit experimental data, even if the model is incorrect, using material parameters that are not necessarily physiologically reasonable. In this study we show that, with an accurate geometrical reconstruction, correct boundary conditions, and material properties based primarily on a priori estimates, a finite-element model of the gerbil middle ear can produce responses that are similar to responses measured in live animals. Two of the important new contributions of this work are that the similarities are based on features of individual responses and not of average responses, and that the similarity of features can be obtained using model parameters mostly based on a priori estimates. This builds confidence in the modelling approach and assumptions.

This study is mainly focused on the TM displacement responses in the frequency domain. We have collected experimental data on TM motions in two preceding studies (Maftoon et al. 2013, 2014) and those data are used to validate the model. We have concentrated here on the frequency range between 0.2 and 10 kHz, as in our experimental data. There were two reasons for selecting this range in our experimental studies: (1) the noise that we had in our experimental vibration data below 200 Hz; and (2) the complications that standing waves may cause in the ear canal at higher frequencies.

One limitation of this study is that we ignored the interaction of the acoustics of the ear canal and middle-ear cavity with the TM: we compared the results of a no-canal, no-cavity model with estimated ideal open-cavity responses based on responses measured with partial openings in the cavity wall (Maftoon et al. 2014). Furthermore, this study does not try to explore the model response in terms of ossicular vibrations in detail: we have presented the displacements of the manubrium along only a single direction and only the piston component of the stapes displacement. Validation of the ossicular motion will require further study, taking into account the 3-D ossicular motions that have been reported by Decraemer et al.

(2007, 2014) as well as the experimental manubrial motion results by Maftoon et al. (2013, 2014). A future study should investigate losses in the middle ear due to radiation impedance and to damping in different middle-ear structures, as well as middle-ear transmission and power flow from the TM to the cochlea.

Sensitivity Analysis. The sensitivity analysis in this paper only considers the uncertainty in the material properties. Funnell and Decraemer (1996) showed that the TM shape also has a substantial effect on the responses, and the morphological variability of other components of the middle ear (e.g., Salih et al. 2012) may also cause substantial differences in behaviour.

N model parameters define an *N*-dimensional space of input parameters. The baseline results are the results of the model at only one point in this *N*-dimensional space. The one-variable-at-a-time sensitivity analysis that we performed here provides response variations in the neighbourhood of the baseline point in the *N*-dimensional space of the parameters. The other points in this space remain unexplored. Furthermore, interactions between parameters, as two or more parameters vary simultaneously (e.g., Qi et al. 2004), are not investigated in the current study. Such interactions can be expected to be small for small parameter changes as used here, but systematic exploration of such interactions should be done, and will be computationally extremely demanding.

Because we wanted to rank the parameters in order of importance in the neighbourhood of the baseline, we varied all of them by the same percentage (±10 %). However, uncertainties in most of the parameters are much more than 10 %. As an example, Soons et al. (2010) reported a variation from the mean Young's modulus of the malleus and incus of about 20 % in a number of measurements in rabbits. For most parameters of the middle-ear model, one can expect even more uncertainty, in part because of questions about experimental methods and artefacts. Some of the parameters that did not show significant effects in this study may affect the responses significantly if the variation range is extended. Figure 17 provides some examples of effects of extended variation ranges on the umbo response. Increasing the damping of the pars tensa from 2×10^{-6} s to 3×10^{-5} s (the damping that we used for the pars flaccida and joints) shifts the frequency of the middle-ear resonance 60 Hz lower, decreases the umbo magnitude at the resonance peak by about 1 dB, and, most importantly, heavily smooths the high-frequency irregularities. It also changes the phase of the response above 3.5 kHz, with a phase change of 50° at 10 kHz. A 50 % decrease in the Young's modulus of the posterior incudal ligament changes the shapes of the high-frequency irregularities in the range of 2.5 to 6 kHz. Figure 17 also shows the umbo response when the Young's modulus of the incudomallear joint is changed from 0.27 to 3 MPa. This value resulted from fitting a line to the high-stretch part of the experimental curve of Zhang and Gan (2011, Fig. 4B, 0.16 to 0.2 mm). It changes the magnitudes at the lowest frequency and at the resonance peak by about 0.8 and 1 dB, respectively. It also smooths the irregularities in the range of 2.5 to 5.8 kHz but introduces rather distinct peaks in the magnitude and phase at about 5.8 kHz. Although the phase of the cochlear input impedance measured by de La Rochefoucauld et al. (2008) and Ravicz et al. (2008) stayed close to zero in the frequency range of this study, the magnitudes were very variable. For example, the magnitude of the average cochlear input impedance shown in Figure 9 of de La Rochefoucauld et al. (2008) varies between 2×10^{10} Pa s/m and 7×10^{10} Pa s/m below 10 kHz. (In the baseline model we used an impedance of 4×10^{10} Pa s/m). Figure 17 shows umbo responses with these two extreme cochlear input impedances. The feature in the umbo response that is most affected by this parameter is the magnitude at the resonance peak. Outside the frequency range of the resonance, this parameter has relatively little effect on the response.

Model Parameters

The baseline material properties used in the present study are largely based on a priori estimates derived from measurements. Although our current model with an isotropic single-layer TM provides acceptable results in the range of experimental observations, the effects of the TM's multiple layers and their presumed orthotropy need to be explored in a future study. The damping parameters are the least well known parameters of the middle ear. In this study we, like many others, have used the Rayleigh damping model, which provides a practical way of dealing with the phenomenon in the middle ear. However, there is no physiological evidence in favour of Rayleigh damping, which is based purely on computational convenience. Other damping models should be explored in subsequent studies.

The Young's modulus of the pars tensa is one the most important parameters of the model. The baseline value that we used here for this parameter is 10 MPa based on the observation by Chole and Kodama (1989) that the collagen fibres are less dense in gerbil than in human. In previous models from our group, in other species, we frequently considered this parameter to be 20 MPa, as have other groups. Changing the baseline pars-tensa Young's modulus here to 20 MPa changes the low-frequency magnitude from 260 to 200 nm/Pa and causes a 220-Hz increase

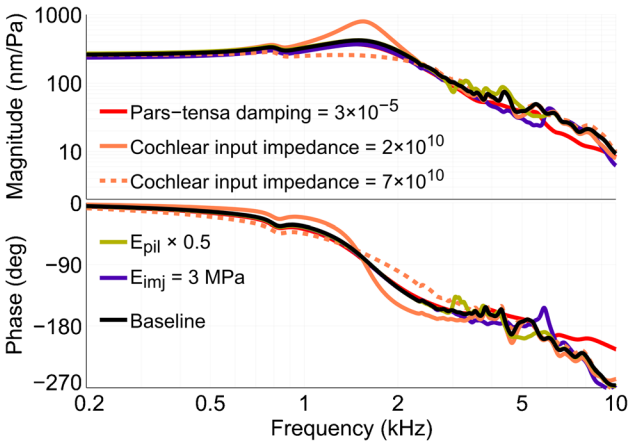

Fig. 17. Umbo responses with baseline parameters and four examples of extended range of variations. *Red* when the damping of the pars tensa is changed to that of the pars flaccida. *Gold* when the Young's modulus of the posterior incudal ligament (E_{pil}) decreased by 50 %. *Violet* when the Young's modulus of the incudomallear joint (E_{imj}) is increased to 3 MPa. *Two orange lines* when the cochlear load was based on the extreme values of the average cochlear input impedance in Figure 9 of de La Rochefoucauld et al. (2008).

in the resonance frequency of the middle ear; the magnitude at the resonance peak decreases by 1.8 dB. Thus, this change causes the model to have a resonance at a frequency slightly higher than what we have measured experimentally but the magnitudes at low frequencies and at the resonance peak stay within the range of experimental observations.

The previous gerbil model from our group (Elkhouri et al. 2006) used a Young's modulus of 60 MPa for the pars tensa. This was based on the value in common between the estimates of Fay et al. (2005) for the posterior section (30–60 MPa) and anterior section (60–90 MPa) of the cat pars tensa. As mentioned earlier ("Pars Tensa" section), because the estimates by Fay et al. were not based on the full thickness of the pars tensa, the resulting high Young's moduli are not really relevant to isotropic models that model the entire thickness of the pars tensa in a single layer. With this value for the Young's modulus of the pars tensa, Elkhouri et al. (2006) calculated a static (low-frequency) displacement of 104 nm/Pa at the umbo. If the Young's modulus of the pars tensa is set to 60 MPa in the present model, which is different from theirs in a number of ways, a very similar low-frequency umbo displacement (100 nm/Pa) is obtained. The focus of the study by Elkhouri et al. was low-frequency behaviour and the Young's modulus of 60 MPa for the pars tensa results in acceptable displacements at low frequencies, at the low end of the range of experimental observations (our Fig. 5). However, the results at higher frequencies are not acceptable; for example, a middle-ear resonance frequency of 2.5 kHz is obtained which is outside the range of experimental observations. The conclusion would be similar for a Young's modulus of 71 MPa, the low end of the range determined for gerbil at low frequencies by Aernouts and Dirckx (2012).

The model with the baseline parameters generates an umbo response that is on the high side of the experimental ranges for the magnitudes at low frequencies and at the middle-ear resonance peak and is somewhat higher than the experimental data at frequencies above middle-ear resonance. Guided by our sensitivity-analysis results, we obtained a preliminary adjusted parameter set that better matches the experimental data. However, this adjusted parameter set may not be optimal. A future study should consider a systematic multi-objective parameter optimization (e.g., Deb 2014), perhaps for the responses of individual ears. This would be computationally expensive.

Our adjusted parameters are not greatly different from the a priori estimates except for the Young's modulus of the joints. This suggests that a better experimental estimate of the Young's modulus of the joints, as well as a more sophisticated treatment of the joints, might be beneficial for the model.

Model Responses

Pars Flaccida and Umbo. The pars flaccida in the model shows responses similar to those measured by Rosowski et al. (1997) and Maftoon et al. (2014). Our sensitivity analysis shows that the resonance of the pars flaccida shifts to lower frequencies as its Young's modulus or thickness decreases. To have a resonance frequency closer to the one from the ear that Rosowski et al. reported, either or both of these two parameters should be decreased. However, this will result in increasing the low-frequency magnitude, which is already in the range of that ear. The model currently has a simplistic treatment of the thickness of the pars flaccida. A model with a variable thickness distribution for the pars flaccida, like what is done for the pars tensa, may provide better results. Since with an open middle-ear cavity the pars flaccida has a very small effect on the motions of the other structures of the middle ear, and because this small effect is limited to a narrow frequency range, we did not try to make the pars-flaccida model more sophisticated.

The model shows that retraction of the pars flaccida into the middle-ear cavity does indeed remove the pars-flaccida feature from the umbo response, in agreement with our experimental study (Maftoon et al. 2013).

The umbo response of the model is within the range of variability seen in the experimental data in terms of the low-frequency magnitude and phase, and of the roll-off slope and irregularities in the response above the resonance frequency. However, with the baseline parameter set, the main resonance frequency and magnitude are on the high side of the experimental range, and for frequencies above the resonance frequency the simulated umbo response is higher than any of the measured responses. The baseline simulated response matches the resonance magnitude and frequency of gerbil I but has heavier damping in that frequency range, more like that of the other gerbils. Although the model with the preliminary adjusted parameters better matches the experimental data at frequencies above the middle-ear resonance, it still shows differences from the experimental results. A more sophisticated model of damping for the pars tensa may improve the results in this regard.

Manubrium. Similar to our experimental observations, the displacement magnitudes along the manubrium increase from the lateral process of the malleus toward the umbo. In our experimental data, we saw a phase difference between the umbo and other manubrial points above 5 kHz. The model results show a noticeable phase difference between about 4.5 and 8 kHz only. The time-domain presentation of the manubrium motion (Fig. 9) shows a rigid-body motion with a fixed axis of rotation at low frequencies. At higher frequencies there is no fixed axis of rotation and a slight bending of the lower half of the manubrium appears. These observations should be further investigated in a future study with a particular focus on ossicular motion.

Pars Tensa. The pars tensa in the model shows behaviour similar to what is seen in experimental ears in terms of (1) the overall magnitudes and phases; (2) the fact that at low frequencies the displacement magnitudes in the posterior region of the pars tensa are larger than those in the anterior region; and (3) the break-up frequency and the bandwidths of the high-frequency response features.

Stapes. Between 5.5 and 6.5 kHz, the stapes response of the model shows minima in both magnitude and phase. In order to make sure that this effect was not caused by having too few elements representing the joint (1434 elements), we refined the mesh of this structure, increasing the number of its elements by a factor of 8. Other than a shift to a slightly higher frequency, no other significant changes happened to this feature after the refinement. Some of the experimental results presented in Figure 12 show similar behaviour in this frequency neighbourhood. Further explorations will be required to understand what causes this feature.

Model Sensitivity

Most features in the model responses do not show significant sensitivity to the parameters of the incus, posterior incudal ligament or stapes. Sensitivity to the malleus stiffness is probably due to the fact that in the gerbil the malleus is attached to the cavity wall at the tip of its anterior process. This very thin bone-to-bone attachment (with no ligament in between) permits rotation of the ossicles because of local deformation of the malleus.

At low frequencies, the responses are dominated by the stiffness-related parameters. The thickness and Young's modulus of the pars tensa and the Young's modulus of the malleus and stapedial annular ligament have the greatest influence on the magnitude of the umbo displacement at low frequencies. The fact that the low-frequency lever ratio remains almost constant as these parameters are varied by ±10 % implies that they also have the most influence on the low-frequency stapes displacement.

Damping of the cochlea mainly affects the sharpness of the middle-ear resonance peak. It has very little effect on the damping of high-frequency vibration features in the pars-tensa responses.

For the magnitude-based features presented in this paper, the model shows antisymmetry with respect to the direction of change of the parameters and their effects; that is, for increases and decreases of the parameters the effects are very similar in magnitude but opposite in sign (corresponding to a linear relationship). Apparent departures from such behaviour in the sensitivity of the frequency-based features are probably affected by the frequency resolution of our analysis and these features probably also show nearly antisymmetric behaviour within the range of ±10 %. Some high-frequency features (not shown in this paper for lack of space) have appeared to demonstrate substantially different behaviour within the ±10 % range and this should be further investigated.

Our analysis shows that, in the neighbourhood close to the baseline parameter set, changes or improvements in the estimates of the material properties of the incus, stapes, incudomallear joint, incudostapedial joint, and posterior incudal ligament will not have large effects on the displacements of the TM and manubrium, nor on displacement of the stapes at frequencies below a few kHz.

ACKNOWLEDGMENTS

The authors would like to thank the editors and the three anonymous reviewers who helped us to improve this paper. This work was supported in part by the Canadian Institutes

of Health Research, the Fonds de recherche en santé du Québec, the Natural Sciences and Engineering Research Council (Canada), the Montréal Children's Hospital Research Institute, the McGill University Health Centre Research Institute and the Research Fund of Flanders (Belgium). Computations were made on the supercomputer Guillimin of McGill University, managed by Calcul Québec and Compute Canada; the operation of this supercomputer is funded by the Canada Foundation for Innovation, NanoQuébec, the Réseau de Médecine Génétique Appliquée and the Fonds de recherche du Québec—Nature et technologies. We thank Clarinda Northrop for providing a collection of gerbil histological slides and Yu Xin Shen for digitizing and cataloguing the collection.

REFERENCES

Aernouts J, Dirckx JJJ (2011) Elastic characterization of the gerbil pars flaccida from in situ inflation experiments. Biomech Model Mechanobiol 10(5):727–741

Aernouts J, Dirckx JJJ (2012) Static versus dynamic gerbil tympanic membrane elasticity: derivation of the complex modulus. Biomech Model Mechanobiol 11(6):829–840

Aernouts J, Soons JAM, Dirckx JJJ (2010) Quantification of tympanic membrane elasticity parameters from in situ point indentation measurements: validation and preliminary study. Hear Res 263(1–2):177–182

Aernouts J, Aerts JRM, Dirckx JJJ (2012) Mechanical properties of human tympanic membrane in the quasi-static regime from in situ point indentation measurements. Hear Res 290(1–2):45–54

Agache PG, Monneur C, Leveque JL, Rigal JD (1980) Mechanical properties and Young's modulus of human skin in vivo. Arch Dermatol Res 269(3):221–232

Beranek LL (1954) Acoustics. Acoust. Soc. Am, New York

Bergevin C, Olson ES (2014) External and middle ear sound pressure distribution and acoustic coupling to the tympanic membrane. J Acoust Soc Am 135(3):1294–1312

Buytaert JAN, Salih WHM, Dierick M, Jacobs P, Dirckx JJJ (2011) Realistic 3D computer model of the gerbil middle ear, featuring accurate morphology of bone and soft tissue structures. J Assoc Res Otolaryngol 12(6):681–696

Cheng T, Dai C, Gan RZ (2007) Viscoelastic properties of human tympanic membrane. Ann Biomed Eng 35(2):305–314

Chole RA, Kodama K (1989) Comparative histology of the tympanic membrane and its relationship to cholesteatoma. Ann Otol Rhinol Laryngol 98(10):761–766

Cohen YE, Bacon CK, Saunders JC (1992) Middle ear development III: morphometric changes in the conducting apparatus of the Mongolian gerbil. Hear Res 62(2):187–193

Daphalapurkar NP, Dai C, Gan RZ, Lu H (2009) Characterization of the linearly viscoelastic behavior of human tympanic membrane by nanoindentation. J Mech Behav Biomed Mater 2(1):82–92

Davies DV (1948) A note on the articulations of the auditory ossicles and related structures. J Laryngol Otol 62(08):533–536

de La Rochefoucauld O, Decraemer WF, Khanna SM, Olson ES (2008) Simultaneous measurements of ossicular velocity and intracochlear pressure leading to the cochlear input impedance in gerbil. J Assoc Res Otolaryngol 9(2):161–177

Deb K (2014) Multi-objective Optimization. In: Burke EK, Kendall G (eds) Search methodologies. Springer, US, pp 403–449

Decraemer WF, Maes MA, Vanhuyse VJ (1980) An elastic stress-strain relation for soft biological tissues based on a structural model. J Biomech 13(6):463–468

Decraemer WF, de Rochefoucauld OL, Dong W, Khanna SM, Dirckx JJJ, Olson ES (2007) Scala vestibuli pressure and three-dimensional stapes velocity measured in direct succession in gerbil. J Acoust Soc Am 121(5):2774–2791

Decraemer WF, Dirckx JJJ, Maftoon N, Funnell WRJ (2010) Simulating large deformations of the gerbil pars flaccida to determine its material properties. 33rd Midwinter Research Meeting. Association for research in otolaryngology, Anaheim

Decraemer WF, Maftoon N, Dirckx JJJ, Funnell WRJ (2011) The effects of the asymmetric shape of the tympanic membrane on the asymmetry of ossicular displacements for positive and negative static pressures. 34th ARO MidWinter Meeting. Retrieved from http://www.aro.org/archives/2011/2011_52_1305771725.html

Decraemer WF, Rochefoucauld de OL, Funnell WRJ, Olson ES (2014) Three-dimensional vibration of the malleus and incus in the living gerbil. J Assoc Res Otolaryngol 1–28. doi:10.1007/s10162-014-0452-1

Elkhouri N, Liu H, Funnell WRJ (2006) Low-frequency finite-element modeling of the gerbil middle ear. J Assoc Res Otolaryngol 7(4):399–411

Fay J, Puria S, Decraemer WF, Steele C (2005) Three approaches for estimating the elastic modulus of the tympanic membrane. J Biomech 38(9):1807–1815

Fay JP, Puria S, Steele CR (2006) The discordant eardrum. Proc Natl Acad Sci 103(52):19743–19748

Ferrazzini M (2003) Virtual middle ear: a dynamic mathematical model based on the finite element method. ETH Zürich. Retrieved from http://cds.cern.ch/record/894552

Fumagalli Z (1949) Ricerche morfologiche sull'apparato di trasmissione del suono. Sound-conducting apparatus: a study of morphology. Istituto per la diffusione di opere scientifiche, Milano

Funnell WRJ (2001) High-frequency time-domain behaviour of a finite-element model of the eardrum. Presented at the 24th Midwinter Research Meeting of the Association for Research in Otolaryngology, St. Petersburg Beach, FL. Retrieved from http://audilab.bme.mcgill.ca/AudiLab/research.html

Funnell WRJ, Decraemer WF (1996) On the incorporation of moiré shape measurements in finite-element models of the cat eardrum. J Acoust Soc Am 100(2):925–932

Funnell WRJ, Laszlo CA (1978) Modeling of the cat eardrum as a thin shell using the finite-element method. J Acoust Soc Am 63:1461

Funnell WRJ, Laszlo CA (1982) A critical review of experimental observations on ear-drum structure and function. ORL 44(4):181–205

Funnell WRJ, Decraemer WF, Khanna SM (1987) On the damped frequency response of a finite-element model of the cat eardrum. J Acoust Soc Am 81:1851

Funnell WRJ, Decraemer WF, Von Unge M, Dirckx JJJ (1999) Finite-element modelling of the gerbil eardrum and middle ear. 22nd ARO MidWinter Meeting. Retrieved from http://www.aro.org/archives/1999/799.html

Funnell WRJ, Decraemer WF, Von Unge M, Dirckx JJJ (2000) Finite-element modelling of the gerbil eardrum and middle ear. 23rd ARO MidWinter Meeting. Retrieved from http://www.aro.org/archives/1999/799.html

Funnell WRJ, Maftoon N, Decraemer WF (2012) Mechanics and modelling for the middle ear. Retrieved March 3, 2013 from http://audilab.bme.mcgill.ca/~funnell/AudiLab/mammie/mammie.pdf

Funnell WRJ, Maftoon N, Decraemer WF (2013) Modeling of middle-ear mechanics. In: Puria S, Fay RR, Popper AN (eds) The middle ear - science, otosurgery, and technology

GAIHEDE M, LIAO D, GREGERSEN H (2007) In vivo areal modulus of elasticity estimation of the human tympanic membrane system: modelling of middle ear mechanical function in normal young and aged ears. Phys Med Biol 52(3):803–814

GAN RZ, YANG F, ZHANG X, NAKMALI D (2011) Mechanical properties of stapedial annular ligament. Med Eng Phys 33(3):330–339

GEA SLR, DECRAEMER WF, FUNNELL RWJ, DIRCKX JJJ, MAIER H (2009) Tympanic membrane boundary deformations derived from static displacements observed with computerized tomography in human and gerbil. J Assoc Res Otolaryngol 11(1):1–17

GEERLIGS M, VAN BREEMEN L, PETERS G, ACKERMANS P, BAAIJENS F, OOMENS C (2011) In vitro indentation to determine the mechanical properties of epidermis. J Biomech 44(6):1176–1181

GENTIL F, JORGE RN, FERREIRA AJM, PARENTE MPL, MOREIRA M, ALMEIDA E (2005) Biomechanical study of middle ear. Proc. COMPLAS VIII (Vol. 2, pp. 785–788). Retrieved from http://congress.cimne.upc.es/complas05/admin/Files/FilePaper/p313.pdf

GEUZAINE C, REMACLE J-F (2009) Gmsh: a 3-D finite element mesh generator with built-in pre- and post-processing facilities. Int J Numer Methods Eng 79(11):1309–1331

GHADARGHADAR N, AGRAWAL SK, SAMANI A, LADAK HM (2013) Estimation of the quasi-static Young's modulus of the eardrum using a pressurization technique. Comput Methods Prog Biomed 110(3):231–239

GREAVES GN, GREER AL, LAKES RS, ROUXEL T (2011) Poisson's ratio and modern materials. Nat Mater 10(11):823–837

HARTY M (1953) Elastic tissue in the middle-ear cavity. J Laryngol Otol 67(12):723–729

HESABGAR SM, MARSHALL H, AGRAWAL SK, SAMANI A, LADAK HM (2010) Measuring the quasi-static Young's modulus of the eardrum using an indentation technique. Hear Res 263(1–2):168–176

HUANG G, GAN RZ, LU H, DAPHALAPURKAR NP (2008) A method for measuring linearly viscoelastic properties of human tympanic membrane using nanoindentation. J Biomech Eng 130(1):014501–014501

KINSLER LE, FREY AR, COPPENS AB, SANDERS JV (1999) FUNDAMENTALS OF ACOUSTICS. WILEY AND SONS, NEW YORK

KIRIKAE I (1960) The structure and function of the middle ear. University of Tokyo Press, Tokyo

KUYPERS LC, DIRCKX JJJ, DECRAEMER WF, TIMMERMANS J-P (2005) Thickness of the gerbil tympanic membrane measured with confocal microscopy. Hear Res 209(1–2):42–52

LADAK HM, FUNNELL WRJ (1996) Finite-element modeling of the normal and surgically repaired cat middle ear. J Acoust Soc Am 100:933

LEE CY, ROSOWSKI JJ (2001) Effects of middle-ear static pressure on pars tensa and pars flaccida of gerbil ears. Hear Res 153(1-2):146–163

LESSER THJ, WILLIAMS KR (1988) The tympanic membrane in cross section: a finite element analysis. J Laryngol Otol 102(03):209–214

LIM DJ (1968A) Tympanic membrane: electron microscopic observation part I: pars tensa. Acta Otolaryngol 66(1-6):181–198

LIM DJ (1968B) Tympanic membrane part II: pars flaccida. Acta Otolaryngol 66(1-6):515–532

LIM DJ (1970) Human tympanic membrane: an ultrastructural observation. Acta Otolaryngol 70(3):176–186

LUO H, DAI C, LU H, GAN RZ (2009) Measurement of Young's modulus of human tympanic membrane at high strain rates. J Biomech Eng 131(6):064501–064501

LYNCH TJI, NEDZELNITSKY V, PEAKE WT (1982) Input impedance of the cochlea in cat. J Acoust Soc Am 72(1):108–130

MAFTOON N, NAMBIAR S, FUNNELL WRJ, DECRAEMER WF, DANIEL SJ (2011) Experimental and modelling study of gerbil tympanic-membrane vibrations. 34th ARO MidWinter Meeting. Retrieved from http://www.aro.org/archives/2011/2011_46_1305771725.html

MAFTOON N, FUNNELL WRJ, DANIEL SJ, DECRAEMER WF (2013) Experimental study of vibrations of gerbil tympanic membrane with closed middle-ear cavity. J Assoc Res Otolaryngol. Accepted.

MAFTOON N, FUNNELL WRJ, DANIEL SJ, DECRAEMER WF (2014) Effect of opening middle-ear cavity on vibrations of gerbil tympanic membrane. J Assoc Res Otolaryngol 15(3):319–334

MOTALLEBZADEH H, CHARLEBOIS M, FUNNELL WRJ (2013) A non-linear viscoelastic model for the tympanic membrane. J Acoust Soc Am 134(6):4427–4434

NEWMARK NM (1959) A method of computation for structural dynamics. J Eng Mech Div 85(7):67–94

NICOLAS G, FOUQUET T (2013) Adaptive mesh refinement for conformal hexahedralmeshes. Finite Elem Anal Des 67:1–12

NUMMELA S (1995) Scaling of the mammalian middle ear. Hear Res 85(1-2):18–30

OVERSTREET EHI, RUGGERO MA (2002) Development of wide-band middle ear transmission in the Mongolian gerbil. J Acoust Soc Am 111:261

QI L, MIKHAEL CS, FUNNELL WRJ (2004) Application of the Taguchi method to sensitivity analysis of a middle-ear finite-element model. Proc 28th Ann Conf Can Med Biol Eng Soc 153–156

RABBITT RD, HOLMES MH (1986) A fibrous dynamic continuum model of the tympanic membrane. J Acoust Soc Am 80(6):1716–1728

RABBITT RD, HOLMES MH (1988) Three-dimensional acoustic waves in the ear canal and their interaction with the tympanic membrane. J Acoust Soc Am 83(3):1064–1080

RAVICZ ME, ROSOWSKI JJ, VOIGT HF (1992) Sound-power collection by the auditory periphery of the Mongolian gerbil *Meriones unguiculatus*. I: middle-ear input impedance. J Acoust Soc Am 92(1):157–177

RAVICZ ME, COOPER NP, ROSOWSKI JJ (2008) Gerbil middle-ear sound transmission from 100 Hz to 60 kHz. J Acoust Soc Am 124:363

ROSOWSKI JJ, LEE CY (2002) The effect of immobilizing the gerbil's pars flaccida on the middle-ear's response to static pressure. Hear Res 174(1-2):183–195

ROSOWSKI JJ, TEOH SW, FLANDERMEYER DT (1997) The effect of the pars flaccida of the tympanic membrane on the ear's sensitivity to sound. In: Lewis ER, Long GR, Lyon RF, Narins PM, Steele CR, Hect-Poiner E (eds) Diversity in auditory mechanics. World Scientific, New Jersey, pp 129–135

ROSOWSKI JJ, RAVICZ ME, TEOH SW, FLANDERMEYER D (1999) Measurements of middle-ear function in the Mongolian gerbil, a specialized mammalian ear. Audiol Neurootol 4(3-4):129–136

SALIH WHM, BUYTAERT JAN, AERTS JRM, VANDERNIEPEN P, DIERICK M, DIRCKX JJJ (2012) Open access high-resolution 3D morphology models of cat, gerbil, rabbit, rat and human ossicular chains. Hear Res 284(1–2):1–5

SIM JH, PURIA S, STEELE CR (2007) Calculation of inertial properties of the malleus-incus complex from micro-CT imaging. J Mech Mater Struct 2:1515–1524

SOONS JA, AERNOUTS J, DIRCKX JJ (2010) Elasticity modulus of rabbit middle ear ossicles determined by a novel micro-indentation technique. Hear Res 263(1-2):33–37

SUN Q, GAN RZ, CHANG KH, DORMER KJ (2002) Computer-integrated finite element modeling of human middle ear. Biomech Model Mechanobiol 1(2):109–122

TEOH SW, FLANDERMEYER DT, ROSOWSKI JJ (1997) Effects of pars flaccida on sound conduction in ears of Mongolian gerbil: acoustic and anatomical measurements. Hear Res 106(1-2):39–65

Timoshenko SP, Woinowsky-Krieger S (1959) Theory of plates and shells (Second.). McGraw-Hill, New York

Tuck-Lee JP, Pinsky PM, Steele CR, Puria S (2008) Finite element modeling of acousto-mechanical coupling in the cat middle ear. J Acoust Soc Am 124:348

Volandri G, Di Puccio F, Forte P, Carmignani C (2011) Biomechanics of the tympanic membrane. J Biomech 44(7):1219–1236

von Békésy G (1960) Experiments in hearing. McGraw-Hill, New York

Wada H, Metoki T, Kobayashi T (1992) Analysis of dynamic behavior of human middle ear using a finite-element method. J Acoust Soc Am 92(6):3157

Wang YC, Lakes RS (2005) Composites with inclusions of negative bulk modulus: extreme damping and negative Poisson's ratio. J Compos Mater 39(18):1645–1657

Zhang X, Gan RZ (2011) Experimental measurement and modeling analysis on mechanical properties of incudostapedial joint. Biomech Model Mechanobiol 10(5):713–726